

Variational Quantum Framework for Partial Differential Equation Constrained Optimization

Amit Surana^{*,‡}, Abeynaya Gnanasekaran^{†,‡}

June 12, 2024

Abstract

We present a novel variational quantum framework for linear partial differential equation (PDE) constrained optimization problems. Such problems arise in many scientific and engineering domains. For instance, in aerodynamics, the PDE constraints are the conservation laws such as momentum, mass and energy balance, the design variables are vehicle shape parameters and material properties, and the objective could be to minimize the effect of transient heat loads on the vehicle or to maximize the lift-to-drag ratio. The proposed framework utilizes the variational quantum linear system (VQLS) algorithm and a black box optimizer as its two main building blocks. VQLS is used to solve the linear system, arising from the discretization of the PDE constraints for given design parameters, and evaluate the design cost/objective function. The black box optimizer is used to select next set of parameter values based on this evaluated cost, leading to nested bi-level optimization structure within a hybrid classical-quantum setting. We present detailed computational error and complexity analysis to highlight the potential advantages of our proposed framework over classical techniques. We implement our framework using the PennyLane library, apply it to a heat transfer optimization problem, and present simulation results using Bayesian optimization as the black box optimizer.

1 Introduction

We present a novel variational quantum framework for optimization problems constrained by linear partial differential equations (PDE). Variational quantum algorithms (VQAs) are hybrid classical-quantum algorithms that have emerged as promising candidates to optimally utilize today’s Noisy Intermediate Scale Quantum (NISQ) devices. VQAs use a quantum subroutine to evaluate the cost/energy function using a shallow parameterized quantum circuit. They provide a versatile framework to tackle a wide variety of problems. As such, they have been successfully used in many applications such as finding ground and excited states of Hamiltonians [1, 2, 3, 4], dynamical quantum simulation [5, 6], combinatorial optimization [7, 8], solving linear systems [9, 10, 11], integer factorization [12], principal component analysis [13, 14, 15] and quantum machine learning [16].

In this work we are interested in the application of the variational quantum linear solver (VQLS) [9], a type of VQA for solving ordinary differential equations (ODEs) and partial differential equations (PDEs) [17, 18, 19, 20]. In this framework the ODEs/PDEs are discretized in space/time and embedded into a system of linear equations. VQLS is then applied to the linear system to obtain the normalized solution and compute observables of interest. While there are no theoretical guarantees associated with VQLS, its query complexity is empirically found to scale polylogarithmically with the size of the linear system [9] and thus could be beneficial over classical linear solvers that have a polynomial scaling. Unlike variational algorithms, fault tolerant quantum algorithms (FTQA) for ODE/PDE simulation have also been proposed and have provable theoretical guarantees/advantages over classical methods. Such FTQA rely either on quantum linear system solver or Hamiltonian simulation framework, see for example [21, 22, 23, 24, 25, 26, 27, 28, 29]. While, such FTQA can be used in our proposed PDE constrained optimization framework, in this paper

^{*}amit.surana@rtx.com, RTX Technology Research Center (RTRC), East Hartford, CT, USA.

[†]abeynaya.gnanasekaran@rtx.com, RTX Technology Research Center (RTRC), Berkeley, CA, USA.

[‡]Both authors contributed equally to this work.

we restrict to a variational setting with a focus on NISQ-era implementation. In particular, we extend the VQLS based ODE/PDE solution framework for linear PDE constrained design optimization problems.

Many science and engineering applications necessitate the solution of optimization problems constrained by physical laws that are described by systems of PDEs. Such problems arise in several domains including aerodynamics, computational fluid dynamics (CFD), material science, computer vision, and inverse problems [30]. For instance in aerodynamic design the PDE constraints are the conservation laws for momentum, mass, and energy, the design variables are aerodynamic shape parameters and material properties, and the objective is to minimize heat transfer or to maximize lift-to-drag ratio. Inverse problems on other hand typically involve calibrating PDE model parameters to match the given measurements. Closed-form solutions are generally unavailable for PDE constrained optimization problems, necessitating the development of numerical methods [31, 32, 30]. A variety of classical gradient-based and gradient-free numerical methods have been developed, and rely on repeated calls to the underlying PDE solver. Since PDE simulations are computationally expensive, using them within the design/optimization loop can become a bottleneck.

To address this challenge we propose a variational quantum framework where a quantum device is used for the computationally demanding PDE simulations and design/optimization is carried out on a classical computer. To best of our knowledge, this is the first work considering the simulation and design problem jointly in the context of quantum algorithms. The main contributions of this work are as follows:

- We formulate a bi-level variational quantum framework for solving linear PDE constrained optimization problems as discussed above. We refer to this as bi-level variational quantum PDE constrained optimization (BVQPCO) framework. Our framework utilizes the VQLS algorithm and a black box classical optimizer as its two main building blocks. VQLS is used to solve the linear system constraints, arising from the discretization of the underlying PDEs, for given design parameters, and evaluate the cost/objective function, while the black box optimizer is used to select the next set of parameter values based on the evaluated cost. Since, VQLS itself involves optimization of the ansatz parameters which parameterize the solution of the linear system, this leads to a sequence of nested bi-level optimization steps within a VQA setting.
- We present detailed computational error analysis for VQLS based solution of linear ODEs under explicit and implicit Euler discretization schemes. Furthermore by combining this error analysis with the empirically known results for query complexity of VQLS, we assess potential utility of our BVQPCO framework over the classical methods.
- We implement the BVQPCO framework using the PennyLane library, apply it to solve a prototypical heat transfer optimization problem, and present simulation results using Bayesian optimization (BO) as the black box optimizer.

The paper is organized as follows. In Sec. 3 we motivate the general structure of PDE constrained design optimization problem through a detailed mathematical formulation of the 1D heat transfer optimization problem. We describe our BVQPCO framework and outline a pseudo-code for its implementation in Sec. 4.1. Sec. 4.2 and 4.3 provide an overview of VQLS and BO, respectively. We present the main results from the complexity analysis of the BVQPCO framework in Sec. 5; detailed proofs are provided in the Appendix. In Sec. 6 we illustrate the BVQPCO framework on the heat transfer optimization problem and provide details on the implementation using the PennyLane library. We finally conclude in Sec. 7 with avenues for future work.

2 Notation

Let $\mathbb{N} = \{1, 2, \dots\}$, \mathbb{R} , and \mathbb{C} be the sets of positive integers, real numbers, and complex numbers respectively. We will denote vectors by small bold letters and matrices by capital bold letters. \mathbf{A}^* and \mathbf{A}' will denote the vector/matrix complex conjugate and vector/matrix transpose, respectively. $Tr(\mathbf{A})$ will denote the trace of a matrix. We will represent an identity matrix of size $s \times s$ by \mathbf{I}_s . Kronecker product will be denoted by \otimes .

If $\mathbf{A} \in \mathbb{R}^{m \times n}$ and $\mathbf{B} \in \mathbb{R}^{p \times q}$, then their Kronecker product is given by

$$\mathbf{C} = \mathbf{A} \otimes \mathbf{B} = \begin{pmatrix} a_{11}\mathbf{B} & \cdots & a_{1n}\mathbf{B} \\ \vdots & \vdots & \vdots \\ a_{m1}\mathbf{B} & \cdots & a_{mn}\mathbf{B} \end{pmatrix}, \quad (1)$$

where, $\mathbf{C} \in \mathbb{R}^{mp \times nq}$.

The standard inner product between two vectors \mathbf{x} and \mathbf{y} will be denoted by $\langle \mathbf{x}, \mathbf{y} \rangle$. The l_p -norm in the Euclidean space \mathbb{R}^n will be denoted by $\|\cdot\|_p, p = 1, 2, \dots, \infty$ and is defined as follows

$$\|\mathbf{x}\|_p = \left(\sum_{j=1}^n |x_j|^p \right)^{1/p}, \quad \mathbf{x} \in \mathbb{R}^n. \quad (2)$$

For the norm of a matrix $\mathbf{A} \in \mathbb{R}^{n \times m}$, we use the induced norm, namely

$$\|\mathbf{A}\|_p = \max_{\mathbf{x} \in \mathbb{R}^m} \frac{\|\mathbf{A}\mathbf{x}\|_p}{\|\mathbf{x}\|_p}. \quad (3)$$

We will use $p = 2$, i.e., l_2 norm for vectors and spectral norm for matrices unless stated otherwise. The spectral radius of a matrix denoted by $\rho(\mathbf{A})$ is defined as

$$\rho(\mathbf{A}) = \max\{|\lambda| : \lambda \text{ eigenvalues of } \mathbf{A}\}. \quad (4)$$

Trace norm of a matrix \mathbf{A} is defined as $\|\mathbf{A}\|_{Tr} = Tr(\sqrt{\mathbf{A}^* \mathbf{A}})$ which is the Schatten q -norms with $q = 1$.

We will use standard bracket notation, i.e. $|\psi\rangle$ and $\langle\psi|$ in representing the quantum states [33]. The inner product between two quantum states $|\psi\rangle$ and $|\phi\rangle$ will be denoted by $\langle\psi|\phi\rangle$. For a vector \mathbf{x} , we denote by $|\mathbf{x}\rangle = \frac{\mathbf{x}}{\|\mathbf{x}\|}$ as the corresponding quantum state. The trace norm $\rho(\psi, \phi)$ between two pure states $|\psi\rangle$ and $|\phi\rangle$ is defined as

$$\rho(\psi, \phi) = \frac{1}{2} \|\ |\phi\rangle\langle\phi| - |\psi\rangle\langle\psi| \|_{Tr} = \sqrt{1 - |\langle\phi|\psi\rangle|^2}. \quad (5)$$

3 PDE Constrained Optimization

We consider a general class of PDE constrained design optimization problems of the form

$$\min_{\mathbf{p}, \mathbf{u}} C_d(\mathbf{u}, \mathbf{p}) \quad (6)$$

$$\text{subject to, } \mathbf{F}(\mathbf{u}, \mathbf{p}, t) = 0, \quad (7)$$

$$g_i(\mathbf{p}) \leq 0, i = 1, \dots, N_e, \quad (8)$$

where, $\mathbf{p} \in \mathbb{R}^{N_p}$ is the vector of design variable (e.g., material type, shape), C_d is the cost function (e.g., heat flux, drag/ lift) and $\mathbf{F}(\mathbf{u}, \mathbf{p}, t)$ are the PDE constraints (e.g., conservation laws, constitutive relations, boundary/ initial conditions) with $\mathbf{u}(\mathbf{x}, t; \mathbf{p})$ being the solution of the PDE defined as a function of space \mathbf{x} and time t for given parameters, and $g_i(\mathbf{p}), i = 1, \dots, N_e$ are constraints on the parameters [34]. Note that \mathbf{F} depends on \mathbf{u} and its partial derivatives in space/time, which we have not explicitly represented in \mathbf{F} for brevity.

In this paper we will restrict \mathbf{F} to arise from linear PDEs. The cost function C_d can in general be non-linear, non-convex and non-smooth. The design variables \mathbf{p} can be mixed, i.e. both continuous and discrete valued. Though the underlying PDE is linear, the constraints $\mathbf{F}(\mathbf{u}, \mathbf{p}, t)$ could involve products of \mathbf{u} and \mathbf{p} making them nonlinear. For numerical purposes, the PDE is discretized in space and/or time and the discretized solution $\mathbf{u} \in \mathbb{R}^N$ (with slight abuse of notation) will be typically a very high dimensional vector, i.e., $N \gg 1$. Thus, in general the optimization problem is computationally challenging to solve.

One popular classical approach to solve PDE constrained optimization is via gradient based methods [31, 32, 30]. For example, the gradient of the cost function C_d w.r.t to \mathbf{p} can be obtained via finite differencing. However, that requires solving the PDE (7) at least $N_p + 1$ times to approximate the derivative of the solution

\mathbf{u} with respect to the parameters. A more efficient approach is via adjoint formulation, where one needs to solve the PDE (7) only one time and an additional adjoint equation to compute the required gradient [31, 32]. However, given that this gradient based approach requires forward simulation(s) for each gradient step, it can be computationally intensive. An alternative approach is surrogate model assisted optimization [35, 36], which has particularly gained significant interest with the recent advances in machine learning [37, 38, 39, 40]. In this approach a surrogate model is trained on the PDE variables calculated with solutions from a PDE solver at several different parameter values. The surrogate model which is computationally cheaper to evaluate than the PDE solver, can then be used for optimization. However, this requires large amount of training data or PDE solves, and the model is only approximate. Another related approach is black box optimization, such as Bayesian optimization (see Section 4.3) where the PDE solver is treated as a black box and surrogate model construction and optimization are accomplished simultaneously by sequentially/adaptively sampling parameters for querying the PDE solver [41, 42, 43].

In all the above mentioned approaches obtaining the PDE solution repeatedly for different parameter values is the computational bottleneck. To alleviate this challenge, we propose to use VQLS based PDE solution, and embed that within a classical black box optimization scheme for design/optimization as discussed above.

3.1 Heat Transfer Optimization Problem Formulation

In high temperature aerodynamic applications such as space reentry vehicles, specially-designed heat-resistant coating layers or materials are applied to protect the vehicle body from excessive heat loading. In such applications it is critical to choose appropriate thickness and material property (thermal diffusivity) of the coating layer. While a thicker coating layer improves the level of insulation, it also makes it more susceptible to thermo-mechanical cracking. Thus, one needs to choose the appropriate material while meeting the thickness constraints. To model this problem we consider a canonical setup of a uniform coating layer applied on a flat plate. The plate is subject to a time-dependent heat flux on one end as shown in Fig. 1.

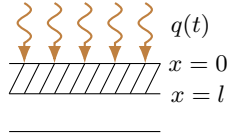


Figure 1: Design of coating layers for a flat plate subject to a time-dependent flux.

To model the heat flow through the plate, we use the 1D heat equation over the domain $[0, l]$ with Neumann boundary conditions

$$\frac{\partial T(x, t)}{\partial t} = \alpha \frac{\partial^2 T(x, t)}{\partial x^2}, \quad (9)$$

$$-k \frac{\partial T(x, t)}{\partial x} \Big|_{x=0} = q(t), \quad (10)$$

$$-k \frac{\partial T(x, t)}{\partial x} \Big|_{x=l} = 0, \quad (11)$$

$$T(x, 0) = T_0(x), \quad (12)$$

where, $t \in [0, P]$, $q(t)$ is time dependent heat flux, k is thermal conductivity, and α is thermal diffusivity. We consider following optimization problem

$$\min_{l, \alpha} C_d(l, \alpha) \equiv \frac{w_1}{P} \int_{t=0}^P \frac{T(l, t) dt}{T_0(l)} + w_2 \left(\frac{l}{l_{\min}} - 1 \right)^2 + w_3 \left(\frac{\alpha}{\alpha_{\max}} - 1 \right)^2, \quad (13)$$

subject to: PDE constraints (9-12),

$$l_{\min} \leq l \leq l_{\max}, \quad \alpha_{\min} \leq \alpha \leq \alpha_{\max},$$

where, $w_i \geq 0, i = 1, 2, 3$ are user selected weights. The optimization problem trades off the thickness l and α with the average temperature at the interface $x = l$.

Discretizing the PDE (9) with second order accuracy in space and the boundary conditions (10) and (11) with first order accuracy in space, the vector $\mathbf{u}(t) = (T_1(t), \dots, T_N(t))'$, where $T_i(t) = T(x_i, t)$, $i = 1, \dots, N$, $x_i = (i-1)\Delta x$ and $\Delta x = \frac{l}{N-1}$, satisfies an ordinary differential equation (ODE)

$$\frac{dT_i(t)}{dt} = \frac{\alpha}{(\Delta x)^2}(T_{i+1} - 2T_i + T_{i-1}),$$

with

$$-k \frac{T_1(t) - T_0(t)}{\Delta x} = q(t), \Rightarrow T_0(t) = \frac{q(t)\Delta x}{k} + T_1(t), \quad (14)$$

$$-k \frac{T_{N+1}(t) - T_N(t)}{\Delta x} = 0, \Rightarrow T_{N+1} = T_N. \quad (15)$$

Therefore, for $i = 1$

$$\frac{dT_1(t)}{dt} = \frac{\alpha}{\Delta x^2}(T_2 - 2T_1 + T_0) = \frac{\alpha}{(\Delta x)^2}(T_2 - T_1) + \frac{\alpha}{k\Delta x}q(t),$$

and, $i = N$

$$\frac{dT_N}{dt} = \frac{\alpha}{(\Delta x)^2}(-T_N + T_{N-1}).$$

Thus one can express the above system of ODEs in a compact vector form as:

$$\frac{d\mathbf{u}}{dt} = \frac{\alpha}{(\Delta x)^2} \mathbf{A} \mathbf{u} + \frac{q(t)}{k\Delta x} \mathbf{e}_1, \quad (16)$$

with the initial condition $\mathbf{u}(0) = \mathbf{u}_0 = (T_0(x_1), \dots, T_0(x_N))'$. Here, $\mathbf{e}_i = (0, \dots, 1, \dots, 0)'$ is the standard unit vector with entry 1 at index i and zero elsewhere and

$$\mathbf{A} = \begin{pmatrix} -1 & 1 & & & 0 \\ 1 & -2 & 1 & & \\ & \ddots & \ddots & \ddots & \\ & & \ddots & -2 & 1 \\ 0 & & & 1 & -1 \end{pmatrix}. \quad (17)$$

3.1.1 Explicit Time Discretization

Furthermore, discretizing the Eqn. (16) in time using the explicit or forward Euler scheme leads to

$$\mathbf{u}_f^{k+1} = \left(\mathbf{I} + \frac{\alpha \Delta t}{(\Delta x)^2} \mathbf{A} \right) \mathbf{u}_f^k + q^k \frac{\Delta t}{k\Delta x} \mathbf{e}_1, \quad k = 1, \dots, M-1$$

where, $\mathbf{u}_f^k = (T_{1k}, T_{2k}, \dots, T_{Nk})'$ with $T_{ik} = T(x_i, t_k)$, $q^k = q((k-1)\Delta t)$, $t_k = (k-1)\Delta t$ and $\Delta t = \frac{P}{M-1}$. Note that for this discretization scheme to be stable, CFL condition should be met $\frac{\alpha \Delta t}{(\Delta x)^2} \leq \frac{1}{2}$.

One can express the set of difference equations above in a form of a single system of linear algebraic equation

$$\tilde{\mathbf{A}}_f \tilde{\mathbf{u}}_f = \tilde{\mathbf{b}}, \quad (18)$$

where, $\tilde{\mathbf{u}}_f = (\mathbf{u}_f^1, \mathbf{u}_f^2, \dots, \mathbf{u}_f^M)'$, $\tilde{\mathbf{b}} = (\mathbf{u}_0, \frac{\Delta t}{k\Delta x} q^1 \mathbf{e}_1, \frac{\Delta t}{k\Delta x} q^2 \mathbf{e}_1, \dots, \frac{\Delta t}{k\Delta x} q^{M-1} \mathbf{e}_1)'$ and

$$\tilde{\mathbf{A}}_f = \begin{pmatrix} \mathbf{I} & 0 & 0 & \dots & 0 \\ -\mathbf{I} - \frac{\alpha \Delta t}{(\Delta x)^2} \mathbf{A} & \mathbf{I} & 0 & 0 & \dots \\ 0 & -\mathbf{I} - \frac{\alpha \Delta t}{(\Delta x)^2} \mathbf{A} & \mathbf{I} & 0 & \dots \\ \vdots & \vdots & \vdots & \dots & \vdots \\ 0 & 0 & \dots & -\mathbf{I} - \frac{\alpha \Delta t}{(\Delta x)^2} \mathbf{A} & \mathbf{I} \end{pmatrix}$$

$$\begin{aligned}
&= \begin{pmatrix} \mathbf{I} & 0 & 0 & \cdots & 0 \\ -\mathbf{I} & \mathbf{I} & 0 & 0 & \cdots \\ 0 & -\mathbf{I} & \mathbf{I} & 0 & \cdots \\ \vdots & \vdots & \vdots & \cdots & \vdots \\ 0 & 0 & \cdots & -\mathbf{I} & \mathbf{I} \end{pmatrix} - \frac{\alpha\Delta t}{(\Delta x)^2} \begin{pmatrix} 0 & 0 & 0 & \cdots & 0 \\ \mathbf{A} & 0 & 0 & 0 & \cdots \\ 0 & \mathbf{A} & 0 & 0 & \cdots \\ \vdots & \vdots & \vdots & \cdots & \vdots \\ 0 & 0 & \cdots & \mathbf{A} & 0 \end{pmatrix} \\
&= \tilde{\mathbf{A}}_{f1} - \frac{\alpha\Delta t}{(\Delta x)^2} \tilde{\mathbf{A}}_{f2}.
\end{aligned} \tag{19}$$

To introduce explicit dependence on l , we define a rescaling $x = ly$, so that $y \in [0, 1]$ and $\Delta x = l\Delta y$, leading to:

$$\begin{aligned}
\tilde{\mathbf{b}}(l, \alpha) &= (\mathbf{u}_0, \frac{\Delta t}{kl\Delta y} q^1 \mathbf{e}'_1, \frac{\Delta t}{kl\Delta y} q^2 \mathbf{e}'_1, \dots, \frac{\Delta t}{kl\Delta y} q^{M-1} \mathbf{e}'_1)', \\
\tilde{\mathbf{A}}_f(l, \alpha) &= \tilde{\mathbf{A}}_{f1} - \frac{\alpha\Delta t}{l^2(\Delta y)^2} \tilde{\mathbf{A}}_{f2}.
\end{aligned}$$

3.1.2 Implicit Time Discretization

Implicit or backward Euler time discretization scheme is unconditionally stable, and leads to

$$\frac{\mathbf{u}_b^{k+1} - \mathbf{u}_b^k}{\Delta t} = \frac{\alpha}{(\Delta x)^2} \mathbf{A} \mathbf{u}_b^{k+1} + q^k \frac{1}{k\Delta x} \mathbf{e}_1,$$

or equivalently

$$\left(I - \frac{\alpha\Delta t}{(\Delta x)^2} \mathbf{A} \right) \mathbf{u}_b^{k+1} = \mathbf{u}_b^k + q^k \frac{\Delta t}{k\Delta x} \mathbf{e}_1.$$

As for the explicit case, we can express the set of difference equations above into a single linear system

$$\tilde{\mathbf{A}}_b \tilde{\mathbf{u}}_b = \tilde{\mathbf{b}}, \tag{20}$$

where, $\tilde{\mathbf{u}}_b$ and $\tilde{\mathbf{b}}$ are similarly defined as above, and

$$\begin{aligned}
\tilde{\mathbf{A}}_b &= \begin{pmatrix} \mathbf{I} & 0 & 0 & \cdots & 0 \\ -\mathbf{I} & (\mathbf{I} - \frac{\alpha\Delta t}{(\Delta x)^2} \mathbf{A}) & 0 & 0 & \cdots \\ 0 & -\mathbf{I} & (\mathbf{I} - \frac{\alpha\Delta t}{(\Delta x)^2} \mathbf{A}) & 0 & \cdots \\ \vdots & \vdots & \vdots & \cdots & \vdots \\ 0 & 0 & \cdots & -\mathbf{I} & (\mathbf{I} - \frac{\alpha\Delta t}{(\Delta x)^2} \mathbf{A}) \end{pmatrix} \\
&= \begin{pmatrix} \mathbf{I} & 0 & 0 & \cdots & 0 \\ -\mathbf{I} & \mathbf{I} & 0 & 0 & \cdots \\ 0 & -\mathbf{I} & \mathbf{I} & 0 & \cdots \\ \vdots & \vdots & \vdots & \cdots & \vdots \\ 0 & 0 & \cdots & -\mathbf{I} & \mathbf{I} \end{pmatrix} - \frac{\alpha\Delta t}{(\Delta x)^2} \begin{pmatrix} 0 & 0 & 0 & \cdots & 0 \\ 0 & \mathbf{A} & 0 & 0 & \cdots \\ 0 & 0 & \mathbf{A} & 0 & \cdots \\ \vdots & \vdots & \vdots & \cdots & \vdots \\ 0 & 0 & \cdots & 0 & \mathbf{A} \end{pmatrix} \\
&= \tilde{\mathbf{A}}_{b1} - \frac{\alpha\Delta t}{(\Delta x)^2} \tilde{\mathbf{A}}_{b2}.
\end{aligned} \tag{21}$$

Similar to the explicit case, one can introduce rescaling with l in the above expression.

3.1.3 Optimization Problem

With these discretizations and rescaling, we can finally express the optimization problem (13) as:

$$\min_{\mathbf{p}, \tilde{\mathbf{u}}_s} C_d(\mathbf{p}, \tilde{\mathbf{u}}_s) \equiv f(\frac{\langle \phi_d, \tilde{\mathbf{u}}_s \rangle}{\langle \phi_n, \tilde{\mathbf{u}}_s \rangle}, \mathbf{p}) = w_1 \frac{\Delta t}{P} \frac{\langle \phi_d, \tilde{\mathbf{u}}_s \rangle}{\langle \phi_n, \tilde{\mathbf{u}}_s \rangle} + w_2 \left(\frac{l}{l_{\min}} - 1 \right)^2 + w_3 \left(\frac{\alpha}{\alpha_{\max}} - 1 \right)^2,$$

$$\text{subject to, } \tilde{\mathbf{A}}_s(\mathbf{p})\tilde{\mathbf{u}}_s = \tilde{\mathbf{b}}(\mathbf{p}) \quad (22)$$

$$l_{\min} \leq l \leq l_{\max}, \quad \alpha_{\min} \leq \alpha \leq \alpha_{\max}, \quad (23)$$

where, $\mathbf{p} = (l, \alpha)$ are the design parameters and we have used the fact that $\int_0^P T(l, t)dt \approx \sum_{k=1}^M T_{Nk}\Delta t$ and $\sum_{k=1}^M T_{Nk} = \langle \phi_d, \tilde{\mathbf{u}}_s \rangle$ for an appropriate choice of vector ϕ_d which picks the locations of $T_{Nk}, k = 1, \dots, M$ from the vector $\tilde{\mathbf{u}}_s$, and ϕ_n is such that $T_0(l) = \langle \phi_n, \tilde{\mathbf{u}}_s \rangle$. The subscript s in $\tilde{\mathbf{u}}_s$ and $\tilde{\mathbf{A}}_s$ can either be f or b depending on the discretization scheme used. Finally, note that even though heat equation is a linear PDE, the constraints (22) are nonlinear in general. Thus, overall the optimization problem involves a quadratic cost function with nonlinear equality and linear inequality constraints, and thus a non-convex problem.

In Sec. 4.1 we propose BVQPCO, a bi-level variational quantum framework to solve the above optimization problem. The VQLS is used to solve the linear system constraint (22) for given parameters l, α , and evaluate the ratio $\frac{\langle \phi_d, \tilde{\mathbf{u}}_s \rangle}{\langle \phi_n, \tilde{\mathbf{u}}_s \rangle}$ required for computing the cost function C_d , while a classical black box optimizer, e.g., Bayesian Optimization (BO) is used to select next set of parameters l, α values based on the evaluated cost. Since, VQLS itself involves optimization of the ansatz parameters which parameterizes the solution of the linear system, this leads to a sequence of nested bi-level optimization steps within a variational setting.

4 Methods

In this section we describe the general BVQPCO framework and provide an overview of VQLS and BO which are its two main building blocks. We also discuss the specific choice of parameters and methods within VQLS/BO for the heat transfer optimization problem discussed in the Sec. 3.1.

4.1 BVQPCO Framework

Following the structure of the PDE constrained optimization problem discussed in the Sec. 3.1, we now consider more general optimization problems of the form

$$\min_{\mathbf{p}, \psi} C_d(\mathbf{p}, \psi) \equiv f \left(\frac{\langle \phi_d, \psi \rangle}{\langle \phi_n, \psi \rangle}, \mathbf{p} \right), \quad (24)$$

$$\text{subject to, } \mathbf{A}(\mathbf{p})\psi = \mathbf{b}(\mathbf{p}), \quad (25)$$

$$g_i(\mathbf{p}) \leq 0, i = 1, \dots, N_e, \quad (26)$$

where, $\mathbf{p} \in R^{N_p}$ are the design/optimization variables, $\psi \in \mathbb{R}^{n_s}$ is the discretized solution vector of the underlying PDE represented in the form of the linear constraints (25), $g_i(\mathbf{p})$ are the constraints on \mathbf{p} , and C_d is the cost function which can be expressed as a function f involving $\phi_d, \phi_n \in \mathbb{R}^{n_s}$ as fixed vectors associated with the cost function.

To solve this problem in a variational quantum framework, we propose BVQPCO framework, where the outer optimization level iteratively selects \mathbf{p}^k using a classical black box optimizer based on the cost function evaluated using solution $|\psi\rangle$ obtained via VQLS for the linear system $\mathbf{A}(\mathbf{p}^k)|\psi\rangle = |\mathbf{b}(\mathbf{p}^k)\rangle$. Thus, the optimization problem (24) can be expressed in a variational quantum form as

$$\min_{\mathbf{p}, \theta} C_d(\mathbf{p}, \theta) \equiv f \left(\frac{\|\phi_d\| \langle \phi_d | \mathbf{V}(\theta) | \mathbf{0} \rangle}{\|\phi_n\| \langle \phi_n | \mathbf{V}(\theta) | \mathbf{0} \rangle}, \mathbf{p} \right), \quad (27)$$

$$\text{subject to, } \mathbf{A}(\mathbf{p})\mathbf{V}(\theta)|\mathbf{0}\rangle = |\mathbf{b}(\mathbf{p})\rangle, \quad (28)$$

$$g_i(\mathbf{p}) \leq 0, i = 1, \dots, N_e, \quad (29)$$

where, $\mathbf{V}(\theta)$ is the VQLS ansatz (see Sec. 4.2) which parametrizes the solution of the linear system (25), and $|\phi_d\rangle, |\phi_n\rangle \in R^{n_s}$ define quantum analogues of the cost function parameters ϕ_d and ϕ_n , respectively. Note that since,

$$\frac{\langle \phi_d, \psi \rangle}{\langle \phi_n, \psi \rangle} = \frac{\|\phi_d\| \langle \frac{\phi_d}{\|\phi_d\|}, \frac{\psi}{\|\psi\|} \rangle}{\|\phi_n\| \langle \frac{\phi_n}{\|\phi_n\|}, \frac{\psi}{\|\psi\|} \rangle} = \frac{\|\phi_d\| \langle \phi_d | \psi \rangle}{\|\phi_n\| \langle \phi_n | \psi \rangle}, \quad (30)$$

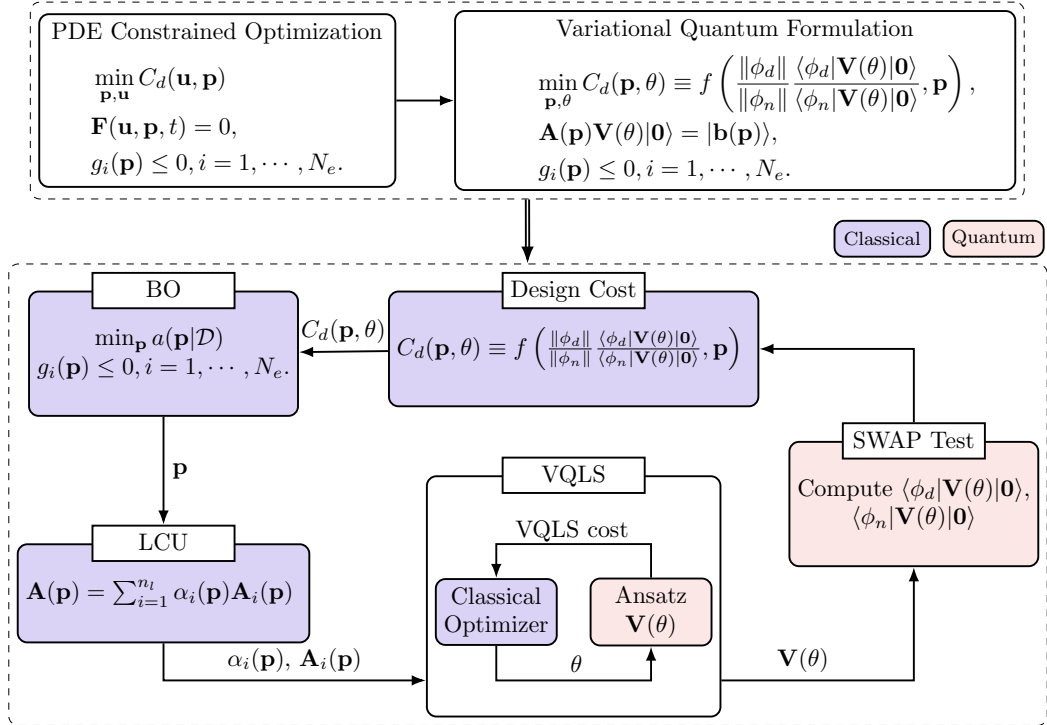


Figure 2: Top: Schematic showing transformation of a PDE constrained optimization problem into a variational quantum form. Bottom: Flow diagram of the BVQPCO framework. VQLS uses an inner level optimization to solve the linear system constraints, arising from the discretization of the underlying PDEs, for given design parameters, and evaluate the quantities related to design cost/objective function. A black box optimizer, e.g., BO is used for the outer level optimization to select next set of parameters values based on the evaluated design cost.

Algorithm 1 BVQPCO Algorithm.

Input: $\mathbf{A}(\mathbf{p})$, $\mathbf{b}(\mathbf{p})$, $|\phi_d\rangle, |\phi_n\rangle$, $\{g_i(\mathbf{p})\}_{i=1}^{N_e}$, $\mathbf{V}(\theta), \gamma, n_{sh}$ and ϵ
Output: Optimal parameters: \mathbf{p}^*

- 1: Initialize $k = 0$ and $\mathbf{p}^0 = \mathbf{p}_{in}$.
- 2: Determine the unitaries $\mathbf{U}_d, \mathbf{U}_n$ which prepare $|\phi_d\rangle$ and $|\phi_n\rangle$, respectively.
- 3: **while** stopping criteria not met **do**
- 4: Compute LCU $\{\alpha_i(\mathbf{p}^k), \mathbf{A}_i(\mathbf{p}^k)\}_{i=1}^{n_k}$ of $\mathbf{A}(\mathbf{p}^k)$, and an unitary \mathbf{U}_b^k such that $|\mathbf{b}(\mathbf{p}^k)\rangle = \mathbf{U}_b^k|\mathbf{0}\rangle$.
- 5: Compute $\theta_*^k = VQLS(\{\alpha_i(\mathbf{p}^k), \mathbf{A}_i(\mathbf{p}^k)\}_{i=1}^{n_k}, \mathbf{U}_b^k, \mathbf{V}(\theta), \gamma, n_{sh})$ using the Algorithm 2.
- 6: Let $|\psi(\theta_*^k)\rangle = \mathbf{V}(\theta_*^k)|\mathbf{0}\rangle$. Compute $\langle\phi_d|\psi(\theta_*^k)\rangle$ and $\langle\phi_n|\psi(\theta_*^k)\rangle$ using associated quantum circuits, and evaluate the cost $C_d^k = f\left(\frac{\langle\phi_d|\psi(\theta_*^k)\rangle}{\langle\phi_n|\psi(\theta_*^k)\rangle}, \mathbf{p}^k\right)$.
- 7: Use classical black box optimizer, e.g. BO Algorithm 3, to select next \mathbf{p}^{k+1} subject to constraints $g_i(\mathbf{p}^{k+1}) \leq 0, i = 0, \dots, N_e$.
- 8: Check the stopping criterion, e.g., whether $S(\mathbf{p}^k, \mathbf{p}^{k+1}) \leq \epsilon$.
- 9: $k \leftarrow k + 1$
- 10: **end while**
- 11: Return \mathbf{p}^k

the cost function (24) can be equivalently expressed in the quantum form (27). Fig. 2 shows the overall flow diagram of the BVQPCO framework. The steps to solve (27) are described in Algorithm 1. Some remarks follow:

- VQLS in the line (5) is implemented as described in the Algorithm 2. The inputs include the linear combination of unitaries (LCU) decomposition of $\mathbf{A}(\mathbf{p})$ (see Sec. 4.2.1), unitary \mathbf{U}_b^k which prepares $|\mathbf{b}(\mathbf{p}^k)\rangle$ (see Sec. 4.2.2), $\mathbf{V}(\theta)$ is the selected ansatz as discussed above (see Sec. 4.2.3), γ is the stopping threshold (see Sec. 4.2.4) and n_{sh} is the number of shots used in VQLS cost function evaluation.
- Depending on how \mathbf{A} depends on the parameters \mathbf{p} , a parameter dependent LCU decomposition $\{\alpha_i(\mathbf{p}), \mathbf{A}_i\}$ can be pre computed once, thus saving computational effort. For instance, for the optimization problem (22), \mathbf{A} for both the explicit (see Eqn. (19)) and implicit (see Eqn. (21)) discretization schemes has a separable structure. Thus, LCU for the matrices $\tilde{\mathbf{A}}_{f1}, \tilde{\mathbf{A}}_{f2}$ (and similarly $\tilde{\mathbf{A}}_{b1}, \tilde{\mathbf{A}}_{b2}$) can be computed once, and the LCU of \mathbf{A} can be readily constructed for any choice of parameters $\mathbf{p} = (l, \alpha)$.
- For computing, $\langle\phi_d|\psi(\theta_*^k)\rangle$ and $\langle\phi_n|\psi(\theta_*^k)\rangle$ in line 6, one can use the circuit associated with SWAP test.
- Note that VQLS provides solution of the given linear system only upto a normalization constant. However, due to the assumed structure of the cost function, it is invariant to the normalization constant as shown by the expression (30). In fact, there is no loss of generality in the assumed form, i.e., $\frac{\langle\phi_d, \psi\rangle}{\langle\phi_n, \psi\rangle}$, as one can always choose $\langle\phi_n, \psi\rangle$ to depend only the initial condition which is known a priori as part of the problem specification.
- For the outer optimization in line (7) one can use any black box optimization method [44]. We propose to use BO (see Sec. 4.3) which is a sequential design strategy for global optimization of black-box functions that does not require derivatives, is robust to noisy evaluation of the cost function, and uses exploration/exploitation trade off to find optimal solution with minimum number of function calls.
- For convergence, line 8 uses a step size tolerance, i.e., $S(\mathbf{p}^k, \mathbf{p}^{k+1}) = \|\mathbf{p}^{k+1} - \mathbf{p}^k\|$. However, other conditions can be employed, such as functional tolerance, i.e. the algorithm is terminated when the change $|C_d^{k+1} - C_d^k|$ is within a specified tolerance ϵ .
- By using VQLS for solving the linear system associated with discretized PDE one can potentially obtain computational advantage over classical methods discussed in the Sec. 3. In the Sec. 5 we provide a detailed computational error analysis for VQLS based solution of linear ODEs. Since, there are no

theoretical results available for query complexity of VQLS, we employ empirically known results along with our rigorous VQLS error analysis to assess potential advantage of the BVQPCO framework over classical methods.

- Note that in the BVQPCO framework one can replace VQLS by a quantum linear system algorithm (QLSA) [45, 46, 47]. This could be beneficial since QLSA have provable exponential advantage over classical linear system solvers. However, since QLSA have high quantum resource needs, incorporating QLSA within our proposed framework may only be feasible in a fault tolerant quantum computing setting.

4.2 Variational Quantum Linear Solver

VQLS is a variational quantum algorithm for solving linear systems of equations on NISQ quantum devices [9]. Given a linear system of the form

$$\mathbf{A}\psi = \mathbf{b}, \quad (31)$$

where, $\mathbf{A} \in R^{N \times N}$ and $\psi, \mathbf{b} \in R^N$, the VQLS finds a normalized $|\psi\rangle$ to fulfill the relationship

$$\mathbf{A}|\psi\rangle = |\mathbf{b}\rangle, \quad (32)$$

where, $|\mathbf{b}\rangle$ denotes the quantum state prepared from the vector \mathbf{b} , and same for $|\psi\rangle$. The inputs to this algorithm are the matrix \mathbf{A} given as a LCU matrices \mathbf{A}_i with the coefficients α_i

$$\mathbf{A} = \sum_{i=1}^{n_i} \alpha_i \mathbf{A}_i, \quad (33)$$

and, a short-depth quantum circuit \mathbf{U}_b for state preparation $|\mathbf{b}\rangle = \mathbf{U}_b|\mathbf{0}\rangle$. Then a cost function $C(\theta)$ is constructed and evaluated with a devised parameterized ansatz $\mathbf{V}(\theta)$. Through the hybrid quantum-classical optimization loop, the optimal parameters θ for the ansatz circuit $\mathbf{V}(\theta)$ can be found such that the cost function $C(\theta)$ achieves the selected convergence criterion. At the end of this feedback loop, the ansatz $\mathbf{V}(\theta_*)$ prepares the quantum state $|\psi_*\rangle = \mathbf{V}(\theta_*)|\mathbf{0}\rangle$ which is proportional to the solution ψ of the linear system (31).

While no theoretical analysis is available, VQLS is empirically found to scale $O((\log N)^{8.5} \kappa \log(1/\epsilon))$ (i.e., polylogarithmically in matrix size N), where κ is the condition number of \mathbf{A} , and ϵ is the desired error tolerance in the solution. Below we summarize comparison of VQLS with classical linear solvers [48]:

- Iterative classical methods like conjugate gradient (CG) scale as $O(Ns\kappa \log(1/\epsilon))$. VQLS is expected to show advantage over CG for large system sizes, $N > 2 \times 10^{12}$ (> 41 qubits) with sparsity $s = 0.5$, precision $\epsilon = 0.01$ and condition number $\kappa = 1$. However, unlike VQLS the CG method is only applicable for positive definite matrices.
- For classical iterative solvers like GMRES (Generalized Minimum Residual Method) which is more general and scales as $O(N^2)$, VQLS would perform better for matrix sizes larger than $N > 2 \times 10^5$ (corresponding to > 17 qubits).
- When we compare VQLS to a direct solver like Gaussian Elimination with $O(N^3)$ complexity we can expect VQLS to show advantage for $N > 750$ (> 9 qubits).

Mainly, VQLS provides an advantage for applications which require only a small part of the full solution vector or only the expectation value of a linear operator acting on the solution vector. Finally, note that like other variational methods, VQLS is plagued by the barren plateau issue which can impose significant computational challenge.

4.2.1 LCU Decomposition

In general, the matrix \mathbf{A} is a non-unitary operator. In order to solve the linear system using VQLS, the matrix is decomposed in terms of unitary operators. One popular approach is based on Pauli basis formed

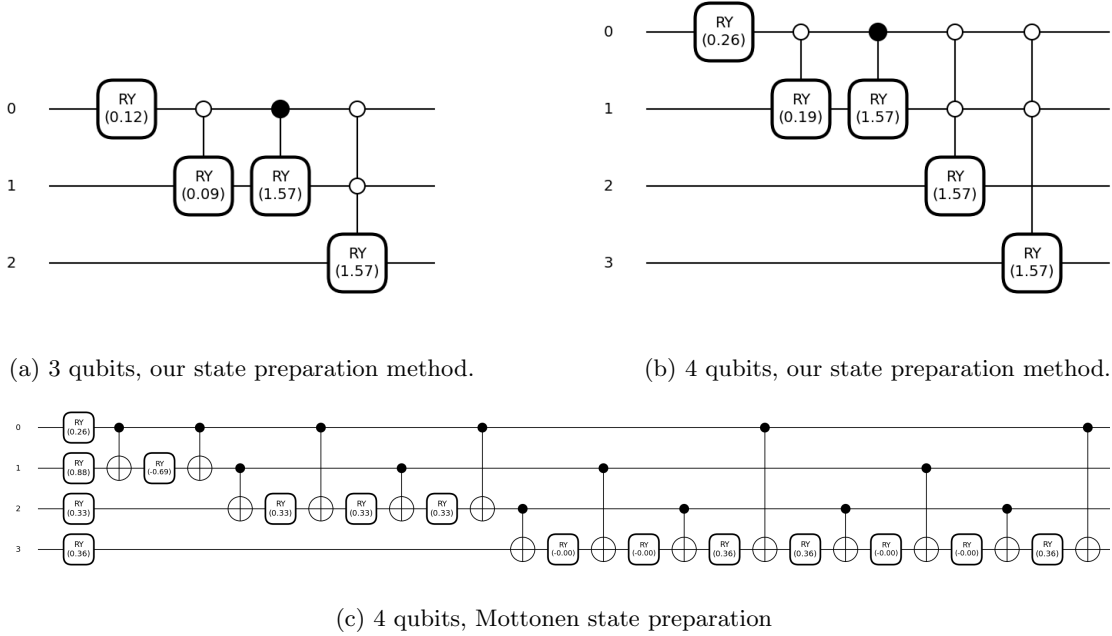


Figure 3: Quantum circuit to prepare state $\tilde{\mathbf{b}}$ in Eqn. (18) with $T_0(x) = 2\left(\frac{\Delta t}{k\Delta x}q^1\right)$, $q^i = q^1 = 50\forall i, k = 1.0, \Delta t = 0.25, \Delta x = 0.2$ (a) 3 qubits, $n_x = 2, n_t = 4$, and (b) 4 qubits $n_x = 4, n_t = 4$. (c) Mottonen state preparation using built-in PennyLane implementation for 4 qubits, $n_x = 4, n_t = 4$ case.

from the identity \mathbf{I} and the Pauli gates \mathbf{X} , \mathbf{Y} and \mathbf{Z} . A matrix \mathbf{A} with the size $2^n \times 2^n$ can be written as a linear combination of elements selected from the basis set

$$P_n = \{\mathbf{P}_1 \otimes \mathbf{P}_2 \cdots \otimes \mathbf{P}_n : \mathbf{P}_i \in \{\mathbf{I}, \mathbf{X}, \mathbf{Y}, \mathbf{Z}\}\}.$$

with complex coefficients α_i as given in Eqn. (33). In this basis, each $\mathbf{A}_i \in P_n$ and its corresponding coefficient α_i can be determined via different approaches [49]. For instance, it can be shown that $\alpha_i = \text{Tr}(\mathbf{A}_i \cdot \mathbf{A})/2^n$. This matrix multiplication based approach can be computationally very expensive. A more efficient approach based on matrix slicing was proposed in [49] and we adapt it in this work. For the matrix in Eqn. (21), the number of terms scale almost linearly with the matrix size. The decomposition has 14 terms for a 8×8 matrix, 26 terms for 16×16 matrix and 54 terms for 32×32 matrix.

4.2.2 State Preparation

A normalized complex vector of a quantum state $|\mathbf{b}\rangle$ is prepared by applying a unitary operation \mathbf{U}_b to the ground state $|\mathbf{0}\rangle$, i.e.

$$|\mathbf{b}\rangle = \mathbf{U}_b|\mathbf{0}\rangle.$$

General purpose methods exist to compute the unitary operator \mathbf{U}_b [50, 51]. However, such methods may not always be efficient and can lead to unnecessarily deep circuits which in turn can affect the performance. Instead, we hand-craft circuits to encode states of form shown in Eqn. (18) using only controlled rotations. Fig. 3(a),(b) show the quantum circuits for the state on 3 and 4 qubits. The rotation angles are computed using user-defined values of the parameters in the state $\tilde{\mathbf{b}}$. In contrast, the quantum circuit for the same state constructed using Mottonen state preparation method is deeper as shown in Fig. 3 (c).

4.2.3 Ansatz Selection

The VQLS employs a parameterized quantum circuit (PQC) or an ansatz which is a gate sequence $\mathbf{V}(\theta)$ which simulates a potential solution $|\psi(\theta)\rangle = \mathbf{V}(\theta)|\mathbf{0}\rangle$. There are variety of choices for ansatz which broadly fall into

the categories of fixed-structure ansatz, problem-specific ansatz, and dynamic/adaptive ansatz [9, 48]. One popular choice of fixed-structure ansatz is the hardware-efficient ansatz (HEA). HEA are designed without taking into account the specific problem being solved, but rather only the topology (backend connectivity of the qubits) and available gates of a specific quantum computer. While these ansatz can be constructed to be more resistant to noise on any specific available quantum device,, they may not be sufficiently expressive and suffer from barren plateau resulting in trainability issue for large scale problems. Problem-specific ansatz does not take into account the specific quantum device being used, and rather tries to exploit the knowledge of the problem available. The Quantum Alternating Operator Ansatz (QAOA) [7] is one such proposed problem-specific ansatz, using two Hamiltonians, known as the driver and the mixer, constructed from specific knowledge of the problem. The requirement of Hamiltonian simulation from the QAOA makes these ansatz far less near-term. In variable structure or dynamic ansatz one optimizes over both the gate parameters θ and the gate placement in the circuit [48].

For real valued problems, such as the example heat transfer optimization problem in Sec. 3.1, the quantum gates used in the ansatz can be restricted appropriately. In this work, we use the fixed structure real-valued ansatz shown in Fig. 4. This is the modified circuit 9 from [52] that was the least expressible with a high KL divergence value of 0.68.

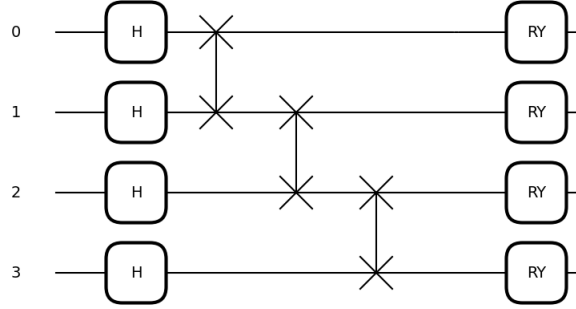


Figure 4: Real-valued ansatz (modified circuit 9) on 4 qubits comprising of Hadamard gate (H), SWAP gates and rotation about y-axis gates (RY).

4.2.4 Cost Function

The VQLS algorithm aims to minimize the cost function $C_{ug}(\theta)$ (or its variant as discussed below)

$$C_{ug}(\theta) = Tr(|\phi\rangle\langle\phi|(\mathbf{I} - |\mathbf{b}\rangle\langle\mathbf{b}|)) = \langle\psi|\mathbf{H}_g|\psi\rangle, \quad (34)$$

where, $|\phi\rangle = \mathbf{A}|\psi(\theta)\rangle$ and

$$\mathbf{H}_g = \mathbf{A}^*\mathbf{U}_b(\mathbf{I} - |\mathbf{0}\rangle\langle\mathbf{0}|)(\mathbf{U}_b)^*\mathbf{A}. \quad (35)$$

$C_{ug}(\theta)$ is large when $|\phi\rangle$ is close to being orthogonal to $|\mathbf{b}\rangle$. Conversely, when $|\phi\rangle$ is nearly proportional to $|\mathbf{b}\rangle$ or small in magnitude, $C_{ug}(\theta)$ is small. The latter case does not represent a true solution. To deal with this, the cost function can be normalized as

$$C_g(\theta) = \frac{C_{ug}}{\langle\phi|\phi\rangle} = 1 - \frac{|\langle\mathbf{b}|\phi\rangle|^2}{\langle\phi|\phi\rangle}. \quad (36)$$

Thus, C_g can be calculated by computing $\langle\mathbf{b}|\phi\rangle$ and $\langle\phi|\phi\rangle$. Given the LCU for the matrix \mathbf{A} and the ansatz $V(\theta)$, this can be accomplished by noting that

$$\langle\phi|\phi\rangle = \sum_{i=1}^{n_l} \sum_{j=1}^{n_l} \beta_{ij} \alpha_i \alpha_j^*, \quad \beta_{ij} = \langle\mathbf{0}|\mathbf{V}^* \mathbf{A}_j^* \mathbf{A}_i \mathbf{V}|\mathbf{0}\rangle, \quad (37)$$

$$|\langle \mathbf{b} | \phi \rangle|^2 = \sum_{i=1}^{n_l} \sum_{j=1}^{n_l} \gamma_{ij} \alpha_i \alpha_j^*, \quad \gamma_{ij} = \langle \mathbf{0} | (\mathbf{U}^b)^* \mathbf{A}_i \mathbf{V} | \mathbf{0} \rangle \langle \mathbf{0} | \mathbf{V}^* \mathbf{A}_j^* \mathbf{U}^b | \mathbf{0} \rangle. \quad (38)$$

There are $n_l(n_l - 1)/2$ different β_{ij} terms which can be estimated using the Hadamard test.

For calculating the terms γ_{ij} , when $i \neq j$, one can compute γ_{ij} by applying Hadamard test to estimate $\langle \mathbf{0} | (\mathbf{U}^b)^* \mathbf{A}_i \mathbf{V} | \mathbf{0} \rangle$ and $\langle \mathbf{0} | \mathbf{V}^* \mathbf{A}_j^* \mathbf{U}^b | \mathbf{0} \rangle$. However, this requires controlling all the unitaries, i.e., $((\mathbf{U}^b)^*, \mathbf{A}_i, \mathbf{V})$. This might be experimentally challenging, especially when the ansatz \mathbf{V} consists of many layers. Instead, Hadamard-Overlap test can be used that directly computes γ_{ij} without having to control \mathbf{V} or \mathbf{U}^b but at the expense of doubling the number of qubits [9]. The terms γ_{ii} can be estimated by applying $(\mathbf{U}^b)^* \mathbf{A}_i \mathbf{V}$ to $|\mathbf{0}\rangle$, and then measuring the probability of the all-zeros outcome.

The global cost functions discussed above can exhibit barren plateaus, i.e., cost function gradients vanish exponentially as a function of number of qubits n . To improve trainability for large n and mitigate the barren plateau issue, the use of local cost function has been proposed. Such unnormalized and normalized local cost functions can be defined as

$$C_{ul}(\theta) = \langle \psi | \mathbf{H}_l | \psi \rangle, \quad C_l(\theta) = \frac{C_{ul}}{\langle \phi | \phi \rangle}, \quad (39)$$

respectively, where the effective Hamiltonian \mathbf{H}_l is

$$\mathbf{H}_l = \mathbf{A}^* \mathbf{U}^b \left(\mathbf{I} - \frac{1}{n} \sum_{k=1}^n |0_k\rangle \langle 0_k| \otimes \mathbf{I}_k \right) (\mathbf{U}^b)^* \mathbf{A}, \quad (40)$$

with $|0_k\rangle$ being a zero state on qubit k , and \mathbf{I}_k being identity on all qubits except the qubit k . Computation of C_l can be accomplished via a slight variation of Hadamard test circuit, see [9] for the details.

Following bounds hold in general for the different cost functions discussed above:

$$C_{ul} \leq C_{ug} \leq n C_{ul}, \quad C_l \leq C_g \leq n C_l,$$

where, $N = 2^n$. Consequently, all cost functions vanish under precisely the same condition, namely $|\phi\rangle \propto |\mathbf{b}\rangle$ and thus consistent with each other. Furthermore, assuming $\|\mathbf{A}\| \leq 1$ the cost functions satisfy (see Lem. 1)

$$C_{ug} \geq \frac{\epsilon^2}{\kappa^2}, \quad C_g \geq \frac{\epsilon^2}{\kappa^2}, \quad C_{ul} \geq \frac{\epsilon^2}{n\kappa^2}, \quad C_l \geq \frac{\epsilon^2}{n\kappa^2}, \quad (41)$$

where, $\epsilon = \rho(\psi, \psi(\theta_*))$ is the error in the normalized solution with $|\psi\rangle$ being the exact solution of Eqn. (32), and $|\psi(\theta_*)\rangle$ being the approximate VQLS solution. These relations can be used in convergence criterion as discussed later.

The global cost function is used for the numerical studies in Sec. 6. Typically, the evaluation of the global cost function is faster than the local cost function as it requires fewer Hadamard/ Hadamard Overlap tests. We found that global cost function performed satisfactorily for the system sizes studied in the work.

4.2.5 Classical Optimizers

There are many different classical optimizers available, both gradient-free and gradient-based, that can be used in VQLS for optimization of the ansatz parameters θ [53]. Gradient-based methods require gradient information during the optimization process, which can either be obtained analytically by a quantum gradient function, or estimated by means of repeated cost function evaluations. Examples include, limited-memory Broyden–Fletcher–Goldfarb–Shanno (L-BFGS), adaptive gradient algorithm (Adagrad), ADAM and AMS-Grad. Gradient-free methods operate as black-box optimizers, which require no extra information besides the values of the cost function evaluations. Examples in this category include, constrained optimization by linear approximation (COBLYA), Nelder-Mead, Modified Powell method, and simultaneous perturbation stochastic approximation (SPSA). We experimented with Adagrad and COBLYA in our numerical studies, see Section 6 for the details.

4.2.6 VQLS Algorithm

The steps for VQLS are summarized in Algorithm 2. To initialize the VQLS iterations (see line (1)) the parameter vector θ_{in} needs to be prescribed. Randomly choosing these parameters with highly likelihood will cause VQLS to start in the region of barren plateau which is not desirable. To overcome these, several other methods for initialization can be employed, see for example [54, 55]. From the relations (41), one can select threshold γ such that, for instance, for $C_g \leq \gamma$, results in approximation error $\epsilon \leq \kappa\sqrt{\gamma \log N}$. The number of shots n_{sh} determines the number of times the quantum circuit is run to estimate each of the term (i.e., β_{ij}, γ_{ij} , see the Sec. 4.2.4) in the cost evaluation. Finally, any of the classical optimizers discussed in the previous section can be used in the Step 4.

Algorithm 2 Outline of VQLS algorithm.

Input: LCU $\{\alpha_i, \mathbf{A}_i\}_{i=1}^{n_l}$, unitary \mathbf{U}_b to prepare $|\mathbf{b}\rangle$, ansatz $\mathbf{V}(\theta)$, convergence threshold γ and number of shots n_{sh} .
Output: Optimal parameters: θ_* .

- 1: Initialize $k = 0$, $\theta^0 = \theta_{in}$ and $c = \infty$.
- 2: **while** $c \geq \gamma$ **do**
- 3: Compute cost $c = C_g(\theta^k)$ using associated quantum circuits with n_{sh} number of shots.
- 4: Use classical optimizer to select next θ^{k+1} .
- 5: $k \leftarrow k + 1$.
- 6: **end while**
- 7: Return θ_k

4.3 Bayesian Optimization

Bayesian optimization (BO) is an approach for global optimization of black box objective functions that take a long time (minutes or hours) to evaluate [56, 57]. Specifically, we consider the following problem:

$$\begin{aligned} & \min_{\mathbf{p}} f(\mathbf{p}) \\ \text{subject to, } & \mathbf{g}(\mathbf{p}) \leq 0, \end{aligned} \quad (42)$$

where, $\mathbf{p} \in \mathbb{R}^{N_p}$ is a parameter vector, $f : \mathbb{R}^{N_p} \rightarrow \mathbb{R}$ is a scalar objective function, and $\mathbf{g} : \mathbb{R}^{N_p} \rightarrow \mathbb{R}^{N_e}$ is the set of N_e constraints. The functional form of f is unknown but we can query a black box function at any point \mathbf{p} and evaluate a noisy value of $f(\mathbf{p})$. The functional form of the constraints \mathbf{g} is assumed to be known.

BO builds a surrogate model for the objective function f and quantifies the uncertainty in that surrogate using a Bayesian machine learning technique. It then uses an acquisition function (AF) defined based on this surrogate to decide where to sample next. This process is repeated till selected convergence criteria are met.

4.3.1 Surrogate Model

The most popular and effective BO relies on a surrogate model in the form of a Gaussian process (GP) due to its flexibility to represent a prior over function. GP is characterized by a prior mean function $\mu_{\beta_m}(\cdot)$ and a covariance function $\kappa_{\beta_k}(\cdot, \cdot)$, where β_m, β_k are the hyperparameters. Consider a finite collection of data pairs $\mathcal{D} = (\mathbf{X}, \mathbf{y})$ of the unknown function $y = f(\mathbf{p}) + \epsilon$ with noise $\epsilon \sim \mathcal{N}(0, \sigma_\epsilon^2(\mathbf{p}))$, where $\mathbf{X} = [\mathbf{p}_1 \ \mathbf{p}_2 \ \cdots \ \mathbf{p}_M]$ are the inputs with corresponding noisy outputs $\mathbf{y} = (y_1, \cdots, y_M)'$ forming the M training samples. The GP model assumes that the observed data are drawn from a multivariate Gaussian distribution \mathcal{N} , and for a new data point \mathbf{p} , the joint distribution of the observed outputs \mathbf{y} and the predicted output y are:

$$\begin{pmatrix} y \\ \mathbf{y} \end{pmatrix} \sim \mathcal{N} \left(\cdot, \begin{pmatrix} \mu_{\beta_m}(\mathbf{p}) \\ \mu_{\beta_m}(\mathbf{X}) \end{pmatrix}, \begin{bmatrix} \kappa_{\beta_k}(\mathbf{p}, \mathbf{p}) & K'_{\beta_k}(\mathbf{X}, \mathbf{p}) \\ K_{\beta_k}(\mathbf{X}, \mathbf{p}) & K_{\beta_k}(\mathbf{X}, \mathbf{X}) + \Sigma_\epsilon \end{bmatrix} \right),$$

where,

- $\mu_{\beta_m}(\mathbf{X}) = [\mu_{\beta_m}(\mathbf{p}_1) \mu_{\beta_m}(\mathbf{p}_2) \cdots \mu_{\beta_m}(\mathbf{p}_M)]'$ in a $M \times 1$ vector,
- $K_{\beta_k}(\mathbf{X}, \mathbf{X}) = [\kappa_{\beta_k}(\mathbf{p}_i, \mathbf{p}_j)]$ is a $M \times M$ correlation matrix evaluated at each pair of the training points,
- $K_{\beta_k}(\mathbf{X}, \mathbf{p}) = [\kappa_{\beta_k}(\mathbf{p}_1, \mathbf{p}) \kappa_{\beta_k}(\mathbf{p}_2, \mathbf{p}) \cdots \kappa_{\beta_k}(\mathbf{p}_M, \mathbf{p})]'$ denotes a $M \times 1$ correlation vector evaluated at all pairs of training and test point,
- and $\Sigma_\epsilon = \text{diag}(\sigma^2(\mathbf{p}_1), \cdots, \sigma^2(\mathbf{p}_M))$ is a diagonal matrix.

The conditional distribution $p(y|\mathbf{p}, \mathbf{X}, \mathbf{y}) \sim \mathcal{N}(\mu(\mathbf{p}), \sigma^2(\mathbf{p}))$ is then a multivariate Gaussian distribution, where the mean and variance of the predicted output y are given by

$$\begin{aligned}\mu(\mathbf{p}) &= \mu_{\beta_m}(\mathbf{p}) + K_{\beta_k}(\mathbf{p}, \mathbf{X})(K_{\beta_k}(\mathbf{X}, \mathbf{X}) + \Sigma_\epsilon)^{-1}(\mathbf{y} - \mu_{\beta_m}(\mathbf{X})), \\ \sigma^2(\mathbf{p}) &= \kappa_{\beta_k}(\mathbf{p}, \mathbf{p}) - K_{\beta_k}'(\mathbf{X}, \mathbf{p})(K_{\beta_k}(\mathbf{X}, \mathbf{X}) + \Sigma_\epsilon)^{-1}K_{\beta_k}(\mathbf{X}, \mathbf{p}),\end{aligned}\quad (43)$$

respectively. Commonly, the mean function $\mu_{\beta_m}(\cdot)$ is taken to be a zero function, and the kernel function is selected as the squared exponential kernel or the Matérn kernel with hyperparameters, such as length scale, signal variance, and noise variance. We will denote by β all the hyperparameters involved. Given the data \mathcal{D} , the optimal hyperparameters β^* are inferred using MLE techniques such as by maximizing the log marginal likelihood. Alternatively, MAP and full Bayesian approaches can also be applied though they tend to be computationally more expensive [58].

4.3.2 Acquisition Function

Given the surrogate, AFs are the utility functions $a(\mathbf{p}|\mathcal{D})$ that guide the search to reach the optimum of the objective function by identifying where to sample next. The guiding principle behind AFs is to strike a balance between exploration and exploitation, which is achieved by querying samples from both known high-fitness-value regions and regions that have not been sufficiently explored so far. Also AF should be computable readily and easy to optimize. Note that any constraints on \mathbf{p} can be incorporated while optimizing the AF, i.e.

$$\begin{aligned}\min_{\mathbf{p}} & a(\mathbf{p}|\mathcal{D}) \\ \text{subject to,} & \quad \mathbf{g}(\mathbf{p}) \leq 0.\end{aligned}\quad (44)$$

Thus, each selected point \mathbf{p}_{M+1} via above optimization is feasible.

Some popular choices of AF include probability of improvement, expected improvement (EI), knowledge gradient, and information theoretic measures, see [57]. We will use EI and its noisy extension for our application. Given the data \mathcal{D} , for noiseless case, i.e. $\epsilon = 0$, EI is defined as

$$a_{EI}(\mathbf{p}|\mathcal{D}) = E_{y \sim \mathcal{N}(\cdot, \mu(\mathbf{p}), \sigma^2(\mathbf{p}))}[\max(0, f^* - y)],$$

where, $f^* = \min\{y_i | y_i \in \mathcal{D}\}$ and $\mu(\mathbf{p})$ and $\sigma(\mathbf{p})$ are as defined in Eqn. (43) with $\Sigma_\epsilon = 0$. This expectation has a closed form expression

$$a_{EI}(\mathbf{p}|\mathcal{D}) = \sigma(\mathbf{p})z\Phi(z) + \sigma(\mathbf{p})\phi(z),\quad (45)$$

where, $z = \frac{f^* - \mu(\mathbf{p})}{\sigma(\mathbf{p})}$, and Φ and ϕ are the cumulative density function and the density function of the standard Normal distribution, respectively. Thus, EI is easy to implement and optimize.

For noisy case $\epsilon \neq 0$, f^* cannot be evaluated exactly since only noisy values of f_i are available. There are various approaches to handle this case. We use the formulation from [59], where EI is replaced by expected EI, defined as:

$$a_{NEI}(\mathbf{p}|\mathcal{D}) = \int_{\mathbf{f}} a_{EI}(\mathbf{p}|\mathcal{D}_{\mathbf{f}})p(\mathbf{f}|\mathcal{D})d\mathbf{f},$$

where, $\mathbf{f} = (f_1, \cdots, f_M)'$, $p(\cdot|\mathcal{D}) = \mathcal{N}(\cdot, \mu_{\beta_m}(\mathbf{X}), K_{\beta_k}(\mathbf{X}, \mathbf{X}) + \Sigma_\epsilon)$ is multivariate Gaussian distribution based on noisy data \mathcal{D} , and $a_{EI}(\mathbf{p}|\mathcal{D}_{\mathbf{f}})$ is evaluated based on a noiseless GP model fitted to data $\mathcal{D}_{\mathbf{f}} = \{(\mathbf{p}_i, f_i)\}$.

This function does not have an analytic expression, but can be estimated using Monte Carlo methods.

Let $K_{\beta_k}(\mathbf{X}, \mathbf{X}) + \Sigma_\epsilon = \mathbf{A}\mathbf{A}'$, e.g., obtained via Cholskey decomposition. Then

$$a_{NEI}(\mathbf{p}|\mathcal{D}) \approx \frac{1}{N_m} \sum_1^{N_m} a_{EI}(\mathbf{p}|\mathcal{D}_{\mathbf{f}_i}),$$

where, $\mathbf{f}_i = \mathbf{A}\Phi^{-1}(\mathbf{s}_i) + \mu_{\beta_m}(\mathbf{X})$ with $\mathbf{s}_i \in [0, 1]^{N_p}$ is a random sample in unit cube of dimension N_p . For sampling \mathbf{s}_i one can use Monte Carlo or Quasi Monte Carlo (QMC) techniques, with latter being preferred as it gives more uniform coverage of the samples. We used a variation of this technique known as the qNoisy EI [60], where the samples are taken from the joint posterior over q test points and the previously observed points.

4.3.3 BO Algorithm

Overall steps of BO algorithm are described in Algorithm 3. In Step 1, N_o QMC samples of input parameters are chosen and the cost function is evaluated N_s times for each sample, to determine the mean and variance of the cost function. In Step 2 MLE is applied to determine GP hyperparameters β , and the GP model is updated in Step 3. The AF is optimized in Step 4 to determine the next sampling point. In Step 5 the black box function is queried N_s times to evaluate mean/variance of the cost function at the new sampling point. Finally, if the convergence criteria are not met in Step 6, the iterations repeat from Step 2. The convergence criteria can be based on stepsize or functional tolerance, similar to as discussed for the VQLS. Finally, note that if the error in evaluating the cost function is negligible, i.e. $\epsilon \approx 0$, there is no need to compute variance in cost function evaluation. Therefore, N_s can be taken to be a single sample, Σ_ϵ is set to be zero in the BO update (43), and the noiseless EI formula (45) can be used for the AF optimization in Step 4.

Algorithm 3 Outline of BO Algorithm.

Input: GP mean/kernel functions and associated parameters β , black box function f , number of initial samples N_o , number of noisy function evaluation N_s , convergence criteria.

Output: Optimal parameters: \mathbf{p}_*

- 1: Randomly select a set of QMC points $\mathbf{p}_i, i = 1, \dots, N_o$. Let $y_{ij}, j = 1 \dots, N_s$ be samples of noisy values of $f(\mathbf{p}_i)$ evaluated at \mathbf{p}_i . Let

$$\bar{y}_i = \frac{1}{N_s} \sum_{j=1}^{N_s} y_{ij}, \quad \Delta_i = \frac{1}{N_s} \sum_{j=1}^{N_s} (y_{ij} - \bar{y}_i)^2,$$

be the estimated mean and variance at \mathbf{p}_i , respectively. Let $\mathcal{D} = \{(\mathbf{p}_i, \bar{y}_i, \Delta_i)\}$.

- 2: Given \mathcal{D} use MLE to infer the prior hyperparameters β .
 - 3: Update the GP posterior mean and covariance using Eqn. (43), with $\Sigma_\epsilon = \text{diag}(\Delta_1, \dots, \Delta_{N_o})$.
 - 4: Optimize the acquisition function $a_{NEI}(\mathbf{p}|\mathcal{D})$ as per (44) and determine next sampling point \mathbf{p}_n .
 - 5: Compute \bar{y}_n and associated Δ_n at \mathbf{p}_n . Augment the data $\mathcal{D} \leftarrow \mathcal{D} \cup \{\mathbf{p}_n, \bar{y}_n, \Delta_n\}$.
 - 6: If convergence criterion not met, go to the Step 2.
-

5 Computational Error and Complexity Analysis

In this section we present a detailed complexity analysis for VQLS based solution of linear ODEs under explicit and implicit Euler discretization schemes, and use that to assess potential advantage of BVQPCO framework over classical techniques. Consider the initial value problem (IVP) for an inhomogeneous system of linear ODEs

$$\begin{aligned} \dot{\mathbf{u}} &= \mathbf{A}\mathbf{u} + \mathbf{b}(t), \\ \mathbf{u}(0) &= \mathbf{u}_0 \in \mathbb{R}^N, \end{aligned} \tag{46}$$

where, $\mathbf{A} \in \mathbb{R}^{N \times N}$, $\mathbf{b}(t) \in \mathbb{R}^N$, $\mathbf{u}(t) \in \mathbb{R}^N$ and $t \in [0, T]$. The above ODE for instance could arise from spatial discretization of a linear PDE, as illustrated in Sec. 3.1. We shall denote by \mathbf{u}_c as the vector of

solution

$$\mathbf{u}_c = \begin{pmatrix} \mathbf{u}(0) \\ \mathbf{u}(h) \\ \vdots \\ \mathbf{u}(h(M-1)) \end{pmatrix}, \quad (47)$$

sampled at $t_k = (k-1)h, k = 1, \dots, M$ for a given sampling step size $h > 0$ and an integer $M > 0$.

Assumption 1. For system (46), we assume

- A1: \mathbf{A} is diagonalisable with eigenvalues $\lambda_i, i = 1, \dots, N$ satisfying

$$\text{Re}(\lambda_i) < 0. \quad (48)$$

Furthermore, if \mathbf{A} has real eigenvalues, the assumption can be relaxed to $\lambda_i \leq 0$.

- A2: $\|\mathbf{b}(t)\| = \sup_{[0,T]} \|\mathbf{b}(t)\|_2$ and $\|\dot{\mathbf{b}}(t)\| = \sup_{[0,T]} \|\dot{\mathbf{b}}(t)\|_2$ are bounded.

We will denote by $\rho(\mathbf{A})$ as the spectral radius of \mathbf{A} , and let $\nu = \|\mathbf{A}\|_2$ be its spectral norm.

Before providing detailed error analysis for VQLS based solution of this IVP, we present two lemmas which will be necessary for the proofs that follow.

Lemma 1. For the linear system (31), following bounds hold for the different VQLS cost functions

$$C_{ug} \geq \frac{\epsilon^2}{\kappa^2}, \quad C_g \geq \frac{\epsilon^2}{\kappa^2 \|\mathbf{A}\|}, \quad C_{ul} \geq \frac{\epsilon^2}{n\kappa^2}, \quad C_l \geq \frac{\epsilon^2}{n\kappa^2 \|\mathbf{A}\|}, \quad (49)$$

where, κ and $N = 2^n$ are the condition number and size of \mathbf{A} in (31) respectively, and ϵ is the error tolerance

$$\epsilon = \rho(\psi, \psi(\theta^*)),$$

with ρ being the trace norm, $|\psi\rangle$ being the exact solution of Eqn. (32), and $|\psi(\theta_*)\rangle$ being the approximate VQLS solution.

The proof of above result can be found in [9].

Lemma 2. The trace norm and l_2 norm between $|\psi\rangle$ and $|\phi\rangle$ are related as follows:

$$\left(1 - \frac{\| |\psi\rangle - |\phi\rangle \|_2^2}{2}\right)^2 + \rho^2(\psi, \phi) = 1. \quad (50)$$

Proof. Without loss of generality, we can write $|\psi\rangle$ in terms of $|\phi\rangle$ and state $|\phi^\perp\rangle$ orthogonal to it as

$$|\psi\rangle = \cos \theta |\phi\rangle + \sin \theta |\phi^\perp\rangle.$$

Then as shown in [61] (see pages 274-275)

$$\rho(\psi, \phi) = |\sin \theta|.$$

Also

$$\| |\psi\rangle - |\phi\rangle \|^2 = 2 - 2 \cos \theta.$$

Finally, using the identity $\cos^2 \theta + \sin^2 \theta = 1$, leads to the desired result (50). \square

Assumption 2. We assume that the query complexity of VQLS scales as $\mathcal{O}(\log^{8.5} N \kappa \log(1/\epsilon))$, where κ is the condition number and N is size of the matrix \mathbf{A} , and ϵ is the desired accuracy of the VQLS solution as described in Lem. 1.

Note that above assumption is based on an empirical scaling study in [9] and no theoretical guarantees are available.

5.1 Error Analysis for VQLS Based Explicit Euler Linear ODE Solver

The application of the forward Euler discretization scheme to the IVP (46) involves following steps.

Step 1: Applying the forward Euler method to the system with step size h yields the difference equation

$$\hat{\mathbf{u}}_f^{k+1} = (\mathbf{I} + \mathbf{A}h)\hat{\mathbf{u}}_f^k + h\mathbf{b}^k, \quad k = 1, \dots, M-1, \quad (51)$$

where, $\hat{\mathbf{u}}_f^k$ approximates $\mathbf{u}(t_k) = \mathbf{u}((k-1)h)$, with $\hat{\mathbf{u}}_f^1 = \mathbf{u}(0) = \mathbf{u}_0$, $\mathbf{b}^k = \mathbf{b}((k-1)h)$ and $M-1 = T/h$. The error introduced by Euler discretization is characterized by Lem. 4.

Step 2: The iterative system (51) can be expressed as a system of linear equations

$$\overbrace{\begin{pmatrix} \mathbf{I} & 0 & 0 & \dots \\ -[\mathbf{I} + \mathbf{A}h] & \mathbf{I} & 0 & \dots \\ 0 & 0 & \ddots & \ddots \\ 0 & 0 & -[\mathbf{I} + \mathbf{A}h] & \mathbf{I} \end{pmatrix}}^{\tilde{\mathbf{A}}_f} \overbrace{\begin{pmatrix} \hat{\mathbf{u}}_f^1 \\ \hat{\mathbf{u}}_f^2 \\ \vdots \\ \hat{\mathbf{u}}_f^M \end{pmatrix}}^{\tilde{\mathbf{u}}_f} = \overbrace{\begin{pmatrix} \mathbf{u}_0 \\ h\mathbf{b}^1 \\ \vdots \\ h\mathbf{b}^{M-1} \end{pmatrix}}^{\tilde{\mathbf{b}}}. \quad (52)$$

In the VQLS framework the linear system (52) is further transformed into the form

$$\tilde{\mathbf{A}}_f |\tilde{\mathbf{u}}_f\rangle = |\tilde{\mathbf{b}}\rangle, \quad (53)$$

where, $|\tilde{\mathbf{b}}\rangle = \tilde{\mathbf{b}}/\|\tilde{\mathbf{b}}\|$ and $|\tilde{\mathbf{u}}_f\rangle = \tilde{\mathbf{u}}_f/\|\tilde{\mathbf{u}}_f\|$ are the normalized vectors. The VLQS algorithm then optimizes the parameter θ of the ansatz $\mathbf{V}(\theta)$ such that

$$\tilde{\mathbf{A}}_f \mathbf{V}(\theta)|\mathbf{0}\rangle = |\tilde{\mathbf{b}}\rangle.$$

The optimal parameter θ_* can be used to prepare a solution $|\bar{\mathbf{u}}_f\rangle = \mathbf{V}(\theta_*)|\mathbf{0}\rangle$ which is an approximation to $|\tilde{\mathbf{u}}_f\rangle$. The approximation error is characterized by the Lem. 1. Fig. 5 shows a schematic of the steps involved in transforming and solving a given PDE using VQLS and the associated variables/approximation errors.

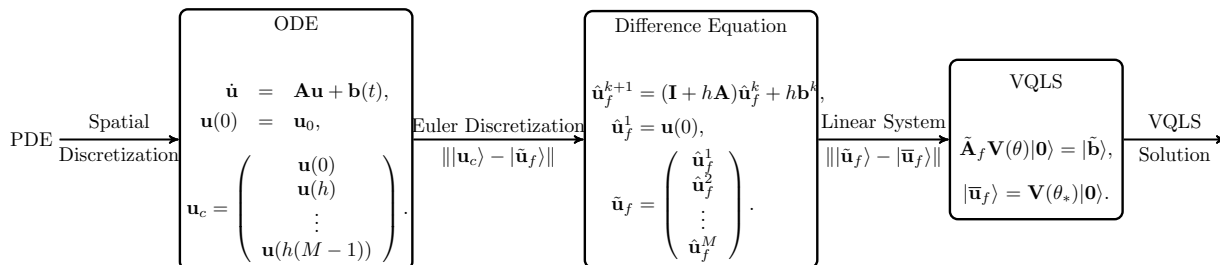


Figure 5: Schematic showing different stages in going from the PDE to the VQLS solution, associated variables and the error in approximations. The case of explicit/forward Euler scheme is shown as an example. Similar flow applies for the case of implicit/backward Euler scheme.

Lemma 3. Let h be chosen such that $h\nu \leq 2$, where $\nu = \|\mathbf{A}\|_2$. Then the stiffness κ of $\tilde{\mathbf{A}}_f$ in (53) is bounded as follows

$$\kappa(\tilde{\mathbf{A}}_f) \leq \frac{12e^{\nu T}}{h\nu}. \quad (54)$$

Lemma 4. Let $\epsilon > 0$ be the desired error, then one can choose the step size h in the forward Euler scheme (51), such that

$$\|\mathbf{u}_c\| - \|\tilde{\mathbf{u}}_f\| \leq \epsilon, \quad (55)$$

where, \mathbf{u}_c is as defined in (47) with this selected h and $|\tilde{\mathbf{u}}_f\rangle$ is solution of the system (53).

See Appendices A.1 and A.2 for proofs of the above two lemmas.

Theorem 1. Consider the IVP (46) under Assumption 1. Let $0 < \epsilon < 1$ be the desired solution accuracy, then one can choose the step size h in the forward Euler scheme (51), and γ the stopping threshold in VQLS Algorithm 2 such that

$$\| |\mathbf{u}_c\rangle - |\bar{\mathbf{u}}_f\rangle \| \leq \epsilon, \quad (56)$$

where, $|\bar{\mathbf{u}}_f\rangle = \mathbf{V}(\theta^*)|\mathbf{0}\rangle$ is solution generated by applying VQLS to the linear system (53). Furthermore, under the Assumption 2 the query complexity scales as

$$\mathcal{O}\left(\log^{8.5}\left(\frac{NT^2}{\|\mathbf{u}_c\|^2\epsilon^2}\right)\frac{Te^{\nu T}}{\|\mathbf{u}_c\|^2\epsilon^2}\log(1/\epsilon)\right). \quad (57)$$

Proof. From Lemmas 4 and 3, we choose h

$$h < \min\left\{\frac{\epsilon^2\|\mathbf{u}_c\|^2}{16C^2T}, \frac{2}{\nu}\right\},$$

such that

$$\| |\mathbf{u}_c\rangle - |\tilde{\mathbf{u}}_f\rangle \| \leq \epsilon/2. \quad (58)$$

Let γ be

$$\gamma = \frac{1 - (1 - \frac{\epsilon^2}{8})^2}{\left(\frac{12e^{\nu T}}{h\nu}\right)^2 (\log(NM))(2 + h\nu)} < 1, \quad (59)$$

where, $N, M > 1$. Let the VQLS algorithm be terminated under the condition (with similar analysis for other VQLS cost functions)

$$C_g \leq \gamma,$$

then from the Lemmas 1 and 3

$$\rho^2(|\tilde{\mathbf{u}}_f\rangle, |\bar{\mathbf{u}}_f\rangle) = (\epsilon')^2 \leq n\kappa^2\|\tilde{\mathbf{A}}_f\|\gamma \leq 1 - \left(1 - \frac{\epsilon^2}{8}\right)^2 \leq \frac{\epsilon^2}{8}\left(2 - \frac{\epsilon^2}{8}\right) \leq \frac{\epsilon^2}{4}, \quad (60)$$

where, the number of qubits $n = \log(NM)$ and we have used the inequality (76). It then follows from Lem. 2

$$1 - \left(1 - \frac{\| |\tilde{\mathbf{u}}_f\rangle - |\bar{\mathbf{u}}_f\rangle \|_2^2}{2}\right)^2 \leq 1 - \left(1 - \frac{\epsilon^2}{8}\right)^2,$$

which implies

$$\| |\tilde{\mathbf{u}}_f\rangle - |\bar{\mathbf{u}}_f\rangle \|_2 \leq \epsilon/2. \quad (61)$$

Thus, using the relations (58) and (61)

$$\| |\mathbf{u}_c\rangle - |\bar{\mathbf{u}}_f\rangle \| \leq \| |\mathbf{u}_c\rangle - |\tilde{\mathbf{u}}_f\rangle \| + \| |\tilde{\mathbf{u}}_f\rangle - |\bar{\mathbf{u}}_f\rangle \| \leq \epsilon. \quad (62)$$

Furthermore, under Assumption 2 the query complexity of VLQS scales as $\mathcal{O}(\log^{8.5}(NM)\kappa\log(1/\epsilon'))$ which can be simplified as follows

$$\begin{aligned} & \mathcal{O}(\log^{8.5}(NM)\kappa\log(1/\epsilon')) = \mathcal{O}\left(\log^{8.5}(NT/h)\frac{e^{\nu T}}{h\nu}\log(1/\epsilon)\right) \\ & = \mathcal{O}\left(\log^{8.5}\left(NT\left(\frac{\nu}{2} + \frac{4C^2T}{\|\mathbf{u}_c\|^2\epsilon^2}\right)\right)e^{\nu T}\left(\frac{1}{2} + \frac{4C^2T}{\|\mathbf{u}_c\|^2\epsilon^2}\right)\log(1/\epsilon)\right) \\ & = \mathcal{O}\left(\log^{8.5}\left(\frac{NT^2}{\|\mathbf{u}_c\|^2\epsilon^2}\right)\frac{Te^{\nu T}}{\|\mathbf{u}_c\|^2\epsilon^2}\log(1/\epsilon)\right). \end{aligned} \quad (63)$$

□

Remark 1. From the estimate of query complexity, one can see that while it scales polylogarithmically with the system size N , there is an exponential dependence on time period of integration, i.e. T . The next theorem shows that under the additional assumption that \mathbf{A} is unitarily diagonalizable (i.e., \mathbf{A} is a normal matrix), the exponential dependence on T reduces to polynomial dependence.

Theorem 2. Consider the IVP (46) under Assumption 1. Additionally, assume that \mathbf{A} in (46) is a normal matrix. Let $0 < \epsilon < 1$ be the desired solution accuracy, then one can choose the step size h in the forward Euler scheme (51), and γ the stopping threshold in VQLS algorithm (2) such that

$$\| |\mathbf{u}_c\rangle - |\bar{\mathbf{u}}_f\rangle \| \leq \epsilon, \quad (64)$$

where, $|\bar{\mathbf{u}}_f\rangle = \mathbf{V}(\theta^*)|\mathbf{0}\rangle$ is solution generated by applying VQLS to the linear system (53). Furthermore, under the Assumption 2 the query complexity scales as

$$\mathcal{O} \left(\log^{8.5} \left(\frac{NT^4}{\|\mathbf{u}_c\|^2 \epsilon^2} \right) \frac{T^3}{\|\mathbf{u}_c\|^2 \epsilon^2} \log(1/\epsilon) \right). \quad (65)$$

The proof is given in Appendix A.3.

Remark 2. The matrix \mathbf{A} (see Eqn. (17)) that arises in the discretization of heat equation is symmetric and hence a normal matrix.

5.1.1 Comparison with Classical Explicit Euler Linear ODE Solver

Given the update eqn. (51), the computational complexity of classical explicit Euler method can be estimated as

$$O(sNM) = O(sNT/h)$$

where, s is sparsity of \mathbf{A} . Following the analysis in Lemma 4, we choose h such that

$$h < \min \left\{ \frac{\epsilon^2 \|\mathbf{u}_c\|^2}{C^2 T}, \frac{2}{\nu} \right\}.$$

Under this condition, the classical Euler approach generates a normalized solution vector $|\tilde{\mathbf{u}}_f^c\rangle$, such that

$$\| |\mathbf{u}_c\rangle - |\tilde{\mathbf{u}}_f^c\rangle \| \leq \epsilon, \quad (66)$$

consistent with the VQLS approach. Thus computational complexity of classical explicit Euler scheme scales as

$$\mathcal{O} \left(sN \frac{T}{h} \right) = \mathcal{O} \left(sNT \left(\frac{\nu}{2} + \frac{C^2 T}{\|\mathbf{u}_c\|^2 \epsilon^2} \right) \right) = \mathcal{O} \left(\frac{sNT^2}{\|\mathbf{u}_c\|^2 \epsilon^2} \right).$$

On the other hand, based on Thm. 1 and 2, the query complexity of VQLS based explicit Euler scheme scales polylogarithmically w.r.t N .

We next discuss implications of this result from the perspective of BVQPCO framework. We assume that, as in BVQPCO framework, an outer optimization loop for design optimization is used with the underlying classical explicit Euler method. Further assuming that number of outer loop iterations are similar in both this classical and the BVQPCO framework, the query complexity of BVQPCO will scale polylogarithmically with N under Assumption 2, and thus could provide a significant computational advantage for simulation based design problems.

5.2 Error Analysis for VQLS Based Implicit Euler Linear ODE Solver

The application of the implicit Euler discretization scheme to the IVP (46) involves following steps.

Step 1: Applying the backward Euler method to the system with step size h yields,

$$(\mathbf{I} - \mathbf{A}h)\hat{\mathbf{u}}_b^{k+1} = \hat{\mathbf{u}}_b^k + h\mathbf{b}^k, \quad k = 1, \dots, M-1, \quad (67)$$

where, $\hat{\mathbf{u}}_b^k$ approximates $\mathbf{u}(t_k) = \mathbf{u}((k-1)h)$, with $\hat{\mathbf{u}}_b^1 = \mathbf{u}(0) = \mathbf{u}_0$, $\mathbf{b}^k = \mathbf{b}((k-1)h)$ and $M-1 = T/h$. The error introduced by Euler discretization is characterized by Lem. 6.

Step 2: The iterative system (67) can be expressed as a system of linear equations,

$$\overbrace{\begin{pmatrix} \mathbf{I} & 0 & 0 & \cdots \\ -\mathbf{I} & [\mathbf{I} - \mathbf{A}h] & 0 & \cdots \\ 0 & 0 & \ddots & \ddots \\ 0 & 0 & -\mathbf{I} & [\mathbf{I} - \mathbf{A}h] \end{pmatrix}}^{\tilde{\mathbf{A}}_b} \overbrace{\begin{pmatrix} \hat{\mathbf{u}}_b^1 \\ \hat{\mathbf{u}}_b^2 \\ \vdots \\ \hat{\mathbf{u}}_b^M \end{pmatrix}}^{\tilde{\mathbf{u}}_b} = \overbrace{\begin{pmatrix} \mathbf{u}_0 \\ h\mathbf{b}^1 \\ \vdots \\ h\mathbf{b}^{M-1} \end{pmatrix}}^{\tilde{\mathbf{b}}}, \quad (68)$$

which in the VQLS framework is further transformed into the form,

$$\tilde{\mathbf{A}}_b |\tilde{\mathbf{u}}_b\rangle = |\tilde{\mathbf{b}}\rangle, \quad (69)$$

where, $|\tilde{\mathbf{u}}_b\rangle = \tilde{\mathbf{u}}_b / \|\tilde{\mathbf{u}}_b\|$ is the normalized vector. We shall denote by $|\bar{\mathbf{u}}_b\rangle = \mathbf{V}(\theta^*)|\mathbf{0}\rangle$, the solution produced by VQLS.

Lemma 5. *Let h be chosen such that $h\nu \leq 0.5$, where $\nu = \|\mathbf{A}\|$. Then the stiffness κ of $\tilde{\mathbf{A}}_b$ in (69) is bounded as follows*

$$\kappa(\tilde{\mathbf{A}}_b) \leq 2.5(T/h + 1), \quad (70)$$

if $\|(\mathbf{I} - h\mathbf{A})^{-1}\| \leq 1$ or

$$\kappa(\tilde{\mathbf{A}}_b) \leq \frac{5e^{2\nu T}}{h\nu}, \quad (71)$$

if $\|(\mathbf{I} - h\mathbf{A})^{-1}\| > 1$.

Lemma 6. *Let $\epsilon > 0$ be the desired error, the one can choose the step size h in implicit Euler scheme (67), such that*

$$\| |\mathbf{u}_c\rangle - |\tilde{\mathbf{u}}_b\rangle \| \leq \epsilon, \quad (72)$$

where, \mathbf{u}_c is as defined in (47) with this selected h and $|\tilde{\mathbf{u}}_b\rangle$ is solution of the system (69).

For the proofs of above two lemmas see Appendices A.4 and A.5.

Theorem 3. *Consider the IVP (46) under the Assumptions 1. Let $0 < \epsilon < 1$ be the desired solution accuracy, then one can choose the step size h in the forward Euler scheme (67), and γ the stopping threshold in VQLS algorithm (2) such that*

$$\| |\mathbf{u}_c\rangle - |\bar{\mathbf{u}}_b\rangle \| \leq \epsilon, \quad (73)$$

where, $|\bar{\mathbf{u}}_b\rangle = \mathbf{V}(\theta_*)|\mathbf{0}\rangle$ is solution generated by applying VQLS to the linear system (69). Furthermore, under Assumption 2 and

- $\|(\mathbf{I} - h\mathbf{A})^{-1}\| \leq 1$, the query complexity scales as

$$\mathcal{O}\left(\log^{8.5}\left(\frac{NT^4}{\|\mathbf{u}_c\|^2\epsilon^2}\right) \frac{T^3}{\|\mathbf{u}_c\|^2\epsilon^2} \log(1/\epsilon)\right). \quad (74)$$

- $\|(\mathbf{I} - h\mathbf{A})^{-1}\| > 1$, the query complexity scales as

$$\mathcal{O}\left(\log^{8.5}\left(\frac{NT^2}{\|\mathbf{u}_c\|^2\epsilon^2}\right) \frac{Te^{2\nu T}}{\|\mathbf{u}_c\|^2\epsilon^2} \log(1/\epsilon)\right). \quad (75)$$

Proof. By using Lem. 5 and 6, and following similar steps as in Thm. 1 and 2, the result follows. \square

Remark 3. *Given the update eqn. (67), the computational complexity of classical implicit Euler method can be estimated as*

$$O(N^2M) = O(N^2T/h),$$

where, we have assumed a GMRES based matrix inversion approach. Following similar analysis as in Sec. 5.1.1, we can conclude that BVQPCO will scale polylogarithmically with N , under Assumption 2, compared to classical approach and thus could provide a significant computational advantage.

6 Numerical Results

In this section, we demonstrate the application of our BVQPCO framework to solve the heat transfer optimization problem described in Sec. 3.1. The problem is discretized on a grid of size $N = 8$ and $\Delta x = \frac{l}{N-1} = 1/7$. We consider the implicit time discretization given in Sec. 3.1.2 with $\Delta t = 0.25s$ and $M = 4$ time steps. The following values of the parameters are used: $q_0 = 50.0, k = 1.0, l_{\min} = 2.0, l_{\max} = 4.0, \alpha_{\min} = 0.2, \alpha_{\max} = 0.3, w_1 = 10.0, w_2 = 1.0, w_3 = 5.0$. There is a gradient in the initial temperature distribution across the grid as shown in Fig. 6 at $t = 0s$. This can be achieved by choosing the rotation angles in the state preparation circuit shown in Fig. 3.

The algorithm was implemented using the PennyLane software framework for quantum computing. PennyLane’s `lightning.qubit` device was used as the simulator, `autograd` interface was used as the automatic differentiation library and the adjoint method was used for gradient computations. We do not consider any device or measurement noise throughout this study. There are several choices of optimizers which can be used with VQLS as discussed in Sec. 4.2.5. We experimented with the Adagrad optimizer from PennyLane with step size of 0.8 in Sec. 6.1 and COBYLA optimizer from SciPy [62] in Sec. 6.2, both of which worked well in our application. The convergence criteria for VQLS was set to a maximum of 150 iterations. The optimizer is initialized randomly with samples taken from the Beta distribution with shape parameters $\alpha = \beta = 0.5$.

The implementation of Bayesian optimization from Ax, BoTorch [60] was used with Ax’s Loop API. Sobol sequences are used to generate ten initial samples in the parameter space and twenty BO iterations are performed. Fixed noise Gaussian process (where noise is provided as an input) is used as the surrogate model and qNoisy EI is used as the acquisition function. While we do not consider device or measurement noise in this work, we use qNoisy EI model to capture the error in estimation of design cost from the inner VQLS optimization loop. We input standard error to the BO model as $\sigma_\epsilon(l, \alpha) \approx c\sqrt{C_g(l, \alpha) \log N}$ using Eqn. (41), where c is a fixed constant we selected empirically.

6.1 Convergence of VQLS

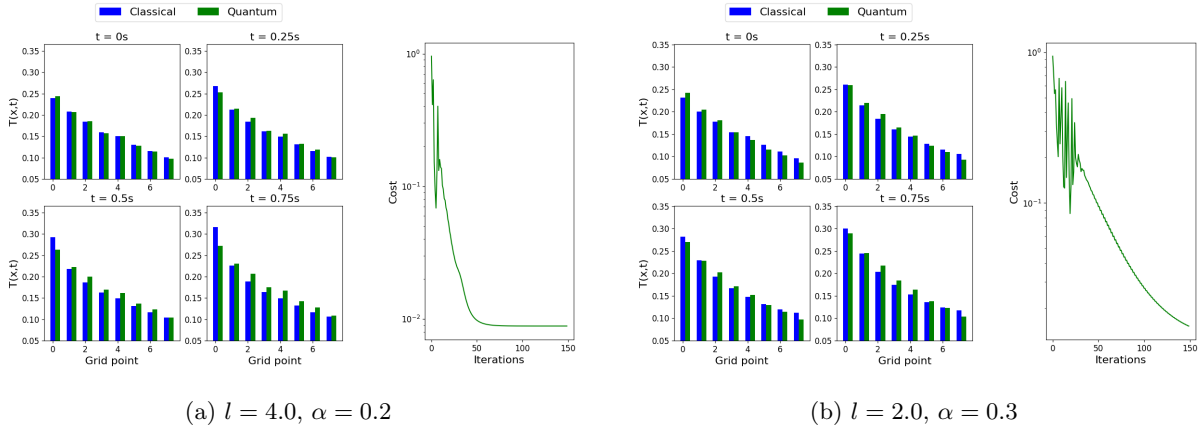
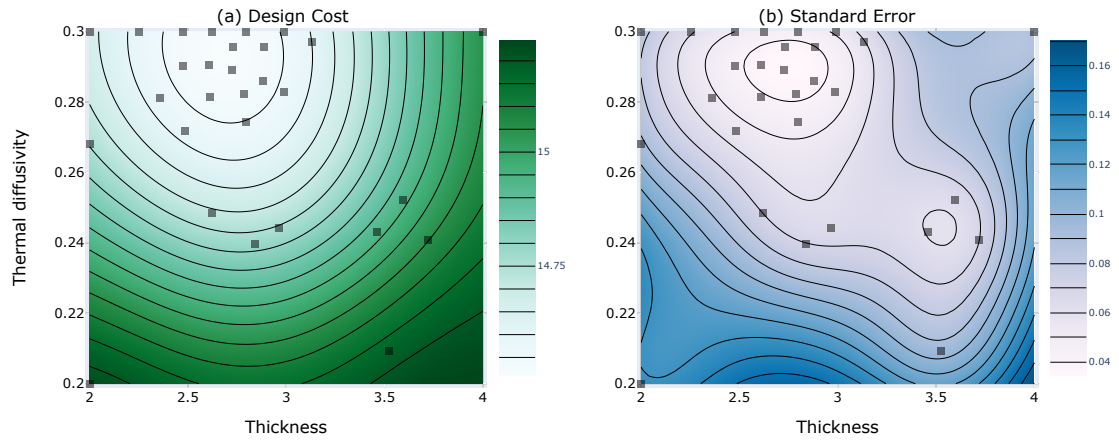


Figure 6: Convergence of VQLS for two different values of the design parameters l, α . The global cost converges to less than 2×10^{-2} within a maximum of 150 iterations.

First, we study the convergence of VQLS for different values of the design parameters l, α . The unitary basis in the LCU decomposition of the $\hat{\mathbf{A}}_{b1}$ and $\hat{\mathbf{A}}_{b2}$ are computed once and the non-zero coefficients are updated using Eqn. (21) for different values of the design parameters. The convergence of VQLS for two set of parameters values is shown in Fig. 6. The quantum solution is compared with the classical solution obtained by solving the linear system (20). Qualitative comparison of the two solutions indicate that VQLS produces reasonable solutions to the problem. In addition, the Adagrad optimizer converges asymptotically to a global cost of less than 2×10^{-2} .



■ In-sample

(c) Model performance

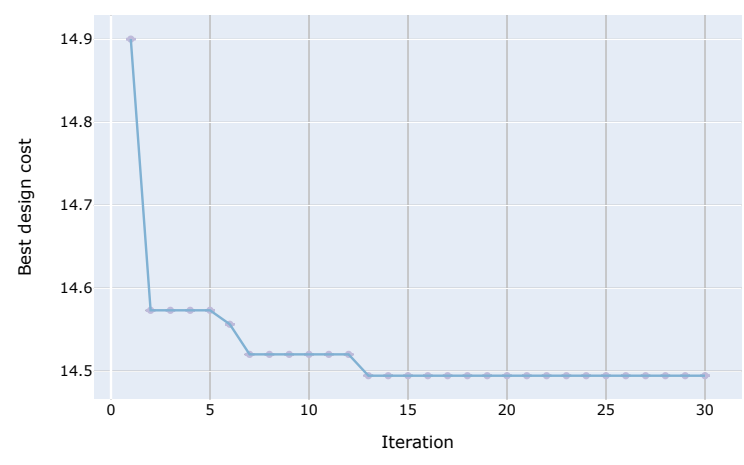


Figure 7: (a) Contour plot illustrating the solution space of the design optimization problem. (b) Contour plot of the standard error in the design cost. c) Performance of the BO model with iteration count.

6.2 Convergence of the BVQPCO framework

Next, we study the performance of the BVQPCO framework on the heat transfer optimization problem (22). The true optimum of the problem is found classically to be $l^* = 2.90$, $\alpha^* = 0.278$. Our algorithm returns the optimal solution as $l = 2.73$ and $\alpha = 0.285$ with less than 0.7% error in the design cost. Fig. 7 shows the convergence of the BO loop. The contour plot in Fig. 7 (a) shows the design cost landscape in the parameter space and the sampled points. Note that more points are concentrated around the optimal point indicating convergence. The standard error shown in Fig. 7 (b) is a combination of the error input to the noisy EI acquisition function and the confidence of the model in predicting the design cost at a given point in the parameter space. Finally, Fig. 7 (c) shows the performance of the model as a function of the iteration count. The best design cost found until a given iteration is plotted on the y-axis. These results demonstrate the overall accuracy and convergence of our BVQPCO framework.

7 Conclusion

In this paper we presented BVQPCO, a novel variational quantum framework for PDE constrained design optimization problems. The proposed framework utilizes the VQLS algorithm and a black box optimizer nested in bi-level optimization structure. We presented a detailed computational error and complexity analysis to establish potential benefits of our framework over classical techniques. We demonstrated the framework on a heat transfer optimization problem and presented simulation results using Bayesian optimization as the black box optimizer. The analysis and results demonstrate the correctness of our framework for solving simulation-based design optimization problems. To the best of our knowledge, this is the first work of its kind in designing a bi-level variational quantum framework for solving PDE constrained design optimization problems.

Future work will involve studying and mitigating the effect of device/ measurement noise and making the BVQPCO framework robust. It will also be worthwhile to study the scalability of the framework by applying it to larger problem sizes and implementing on quantum hardware. One of the bottlenecks in the BVQPCO framework is the computation of VQLS cost function which scales polynomially with the number of LCU terms. We can employ a more efficient tensor product decomposition [63], which exploits the underlying structure and sparsity of matrices such as arising from PDE discretizations, to provide an exponential speed-up in the VQLS cost evaluation. An adaptive multigrid strategy to accelerate convergence of variational quantum algorithms was recently proposed in [64]. Such techniques can be adapted in the context of VQLS to further improve our framework and scale to larger problem sizes. By leveraging Carleman linearization based embedding approach [26, 28] we also plan to extend our framework for nonlinear PDE constrained optimization problems. Finally, adapting the proposed framework for fault tolerant quantum computing setting is also an avenue for future research.

8 Acknowledgments

This research was developed with funding from the Defense Advanced Research Projects Agency (DARPA). The views, opinions, and/or findings expressed are those of the author(s) and should not be interpreted as representing the official views or policies of the Department of Defense or the U.S. Government.

References

- [1] Alberto Peruzzo, Jarrod McClean, Peter Shadbolt, Man-Hong Yung, Xiao-Qi Zhou, Peter J Love, Alán Aspuru-Guzik, and Jeremy L O'brien. A variational eigenvalue solver on a photonic quantum processor. *Nature communications*, 5(1):4213, 2014.
- [2] Ken M Nakanishi, Kosuke Mitarai, and Keisuke Fujii. Subspace-search variational quantum eigensolver for excited states. *Physical Review Research*, 1(3):033062, 2019.
- [3] Tyson Jones, Suguru Endo, Sam McArdle, Xiao Yuan, and Simon C Benjamin. Variational quantum algorithms for discovering hamiltonian spectra. *Physical Review A*, 99(6):062304, 2019.

- [4] Tyson Jones, Suguru Endo, Sam McArdle, Xiao Yuan, and Simon C Benjamin. Variational quantum algorithms for discovering hamiltonian spectra. *Physical Review A*, 99(6):062304, 2019.
- [5] Ying Li and Simon C. Benjamin. Efficient variational quantum simulator incorporating active error minimization. *Phys. Rev. X*, 7:021050, Jun 2017.
- [6] Cristina Cirstoiu, Zoe Holmes, Joseph Iosue, Lukasz Cincio, Patrick J Coles, and Andrew Sornborger. Variational fast forwarding for quantum simulation beyond the coherence time. *npj Quantum Information*, 6(1):82, 2020.
- [7] Edward Farhi, Jeffrey Goldstone, and Sam Gutmann. A quantum approximate optimization algorithm, 2014.
- [8] Edward Farhi and Aram W Harrow. Quantum supremacy through the quantum approximate optimization algorithm. *arXiv preprint arXiv:1602.07674*, 2016.
- [9] Carlos Bravo-Prieto, Ryan LaRose, Marco Cerezo, Yigit Subasi, Lukasz Cincio, and Patrick J Coles. Variational quantum linear solver. *arXiv preprint arXiv:1909.05820*, 2019.
- [10] Xiaosi Xu, Jinzhao Sun, Suguru Endo, Ying Li, Simon C. Benjamin, and Xiao Yuan. Variational algorithms for linear algebra. *Science Bulletin*, 66(21):2181–2188, November 2021.
- [11] Hsin-Yuan Huang, Kishor Bharti, and Patrick Rebentrost. Near-term quantum algorithms for linear systems of equations. *arXiv preprint arXiv:1909.07344*, 2019.
- [12] Eric Anschuetz, Jonathan Olson, Alán Aspuru-Guzik, and Yudong Cao. Variational quantum factoring. In *Quantum Technology and Optimization Problems: First International Workshop, QTOP 2019, Munich, Germany, March 18, 2019, Proceedings 1*, pages 74–85. Springer, 2019.
- [13] Seth Lloyd, Masoud Mohseni, and Patrick Rebentrost. Quantum principal component analysis. *Nature Physics*, 10(9):631–633, 2014.
- [14] Ryan LaRose, Arkin Tikku, Étude O’Neel-Judy, Lukasz Cincio, and Patrick J Coles. Variational quantum state diagonalization. *npj Quantum Information*, 5(1):57, 2019.
- [15] M Cerezo, Kunal Sharma, Andrew Arrasmith, and Patrick J Coles. Variational quantum state eigensolver. *npj Quantum Information*, 8(1):113, 2022.
- [16] Jacob Biamonte, Peter Wittek, Nicola Pancotti, Patrick Rebentrost, Nathan Wiebe, and Seth Lloyd. Quantum machine learning. *Nature*, 549(7671):195–202, 2017.
- [17] YY Liu, Zhen Chen, Chang Shu, Siou Chye Chew, Boo Cheong Khoo, Xiang Zhao, and YD Cui. Application of a variational hybrid quantum-classical algorithm to heat conduction equation and analysis of time complexity. *Physics of Fluids*, 34(11), 2022.
- [18] Reuben Demirdjian, Daniel Gunlycke, Carolyn A Reynolds, James D Doyle, and Sergio Tafur. Variational quantum solutions to the advection–diffusion equation for applications in fluid dynamics. *Quantum Information Processing*, 21(9):322, 2022.
- [19] Hai-Ling Liu, Yu-Sen Wu, Lin-Chun Wan, Shi-Jie Pan, Su-Juan Qin, Fei Gao, and Qiao-Yan Wen. Variational quantum algorithm for the poisson equation. *Physical Review A*, 104(2):022418, 2021.
- [20] Fong Yew Leong, Wei-Bin Ewe, and Dax Enshan Koh. Variational quantum evolution equation solver. *Scientific Reports*, 12(1):10817, 2022.
- [21] Dominic W Berry, Andrew M Childs, Aaron Ostrander, and Guoming Wang. Quantum algorithm for linear differential equations with exponentially improved dependence on precision. *Communications in Mathematical Physics*, 356(3):1057–1081, 2017.
- [22] Xiangyu Li, Xiaolong Yin, Nathan Wiebe, Jaehun Chun, Gregory K Schenter, Margaret S Cheung, and

- Johannes Mülmenstädt. Potential quantum advantage for simulation of fluid dynamics. *arXiv preprint arXiv:2303.16550*, 2023.
- [23] Ryan Babbush, Dominic W Berry, Robin Kothari, Rolando D Somma, and Nathan Wiebe. Exponential quantum speedup in simulating coupled classical oscillators. *Physical Review X*, 13(4):041041, 2023.
- [24] David Jennings, Matteo Lostaglio, Robert B Lowrie, Sam Pallister, and Andrew T Sornborger. The cost of solving linear differential equations on a quantum computer: fast-forwarding to explicit resource counts. *arXiv preprint arXiv:2309.07881*, 2023.
- [25] Andrew M Childs, Jin-Peng Liu, and Aaron Ostrander. High-precision quantum algorithms for partial differential equations. *Quantum*, 5:574, 2021.
- [26] Jin-Peng Liu, Herman Øie Kolden, Hari K Krovi, Nuno F Loureiro, Konstantina Trivisa, and Andrew M Childs. Efficient quantum algorithm for dissipative nonlinear differential equations. *Proceedings of the National Academy of Sciences*, 118(35):e2026805118, 2021.
- [27] Shi Jin, Nana Liu, and Yue Yu. Quantum simulation of partial differential equations via Schrodingerisation: technical details. *arXiv preprint arXiv:2212.14703*, 2022.
- [28] Amit Surana, Abeynaya Gnanasekaran, and Tuhin Sahai. An efficient quantum algorithm for simulating polynomial dynamical systems. *Quantum Information Processing*, 23(3):1–22, 2024.
- [29] Abeynaya Gnanasekaran, Amit Surana, and Tuhin Sahai. Efficient quantum algorithms for nonlinear stochastic dynamical systems. In *2023 IEEE International Conference on Quantum Computing and Engineering (QCE)*, volume 2, pages 66–75. IEEE, 2023.
- [30] Harbir Antil, Drew P Kouri, Martin-D Lacasse, and Denis Ridzal. *Frontiers in PDE-constrained Optimization*, volume 163. Springer, 2018.
- [31] Lorenz T Biegler, Omar Ghattas, Matthias Heinkenschloss, and Bart van Bloemen Waanders. Large-scale pde-constrained optimization: an introduction. In *Large-scale PDE-constrained optimization*, pages 3–13. Springer, 2003.
- [32] Michael Hinze, René Pinnau, Michael Ulbrich, and Stefan Ulbrich. *Optimization with PDE constraints*, volume 23. Springer Science & Business Media, 2008.
- [33] Michael A Nielsen and Isaac L Chuang. *Quantum computation and quantum information*. Cambridge university press, 2010.
- [34] Juan Carlos De los Reyes. *Numerical PDE-constrained optimization*. Springer, 2015.
- [35] Ping Jiang, Qi Zhou, Xinyu Shao, Ping Jiang, Qi Zhou, and Xinyu Shao. *Surrogate-model-based design and optimization*. Springer, 2020.
- [36] Charles Audet, J Denni, Douglas Moore, Andrew Booker, and Paul Frank. A surrogate-model-based method for constrained optimization. In *8th symposium on multidisciplinary analysis and optimization*, page 4891, 2000.
- [37] Physics-informed neural networks: A deep learning framework for solving forward and inverse problems involving nonlinear partial differential equations. *Journal of Computational physics*, 378:686–707, 2019.
- [38] Shengze Cai, Zhiping Mao, Zhicheng Wang, Minglang Yin, and George Em Karniadakis. Physics-informed neural networks (pinns) for fluid mechanics: A review. *Acta Mechanica Sinica*, 37(12):1727–1738, 2021.
- [39] Yubiao Sun, Ushnish Sengupta, and Matthew Juniper. Physics-informed deep learning for simultaneous surrogate modeling and pde-constrained optimization of an airfoil geometry. *Computer Methods in Applied Mechanics and Engineering*, 411:116042, 2023.

- [40] Lu Lu, Raphael Pestourie, Wenjie Yao, Zhicheng Wang, Francesc Verdugo, and Steven G Johnson. Physics-informed neural networks with hard constraints for inverse design. *SIAM Journal on Scientific Computing*, 43(6):B1105–B1132, 2021.
- [41] Yuki Morita, Saleh Rezaeiravesh, Narges Tabatabaei, Ricardo Vinuesa, Koji Fukagata, and Philipp Schlatter. Applying bayesian optimization with gaussian process regression to computational fluid dynamics problems. *Journal of Computational Physics*, 449:110788, 2022.
- [42] Soumalya Sarkar, Sudepta Mondal, Michael Joly, Matthew E Lynch, Shaunak D Bopardikar, Ranadip Acharya, and Paris Perdikaris. Multifidelity and multiscale bayesian framework for high-dimensional engineering design and calibration. *Journal of Mechanical Design*, 141(12):121001, 2019.
- [43] Mike Diessner, Joseph O’Connor, Andrew Wynn, Sylvain Laizet, Yu Guan, Kevin Wilson, and Richard D Whalley. Investigating bayesian optimization for expensive-to-evaluate black box functions: Application in fluid dynamics. *Frontiers in Applied Mathematics and Statistics*, 8:1076296, 2022.
- [44] Stéphane Alarie, Charles Audet, Aïmen E Gheribi, Michael Kokkolaras, and Sébastien Le Digabel. Two decades of blackbox optimization applications. *EURO Journal on Computational Optimization*, 9:100011, 2021.
- [45] Danial Dervovic, Mark Herbster, Peter Mountney, Simone Severini, Naïri Usher, and Leonard Wossnig. Quantum linear systems algorithms: a primer. *arXiv preprint arXiv:1802.08227*, 2018.
- [46] Aram W Harrow, Avinatan Hassidim, and Seth Lloyd. Quantum algorithm for linear systems of equations. *Physical review letters*, 103(15):150502, 2009.
- [47] Pedro CS Costa, Dong An, Yuval R Sanders, Yuan Su, Ryan Babbush, and Dominic W Berry. Optimal scaling quantum linear-systems solver via discrete adiabatic theorem. *PRX quantum*, 3(4):040303, 2022.
- [48] Hrushikesh Patil, Yulun Wang, and Predrag S Krstić. Variational quantum linear solver with a dynamic ansatz. *Physical Review A*, 105(1):012423, 2022.
- [49] Lukas Hantzko, Lennart Binkowski, and Sabhyata Gupta. Tensorized pauli decomposition algorithm. *arXiv preprint arXiv:2310.13421*, 2023.
- [50] Vivek V Shende, Stephen S Bullock, and Igor L Markov. Synthesis of quantum logic circuits. In *Proceedings of the 2005 Asia and South Pacific Design Automation Conference*, pages 272–275, 2005.
- [51] Mikko Mottonen, Juha J Vartiainen, Ville Bergholm, and Martti M Salomaa. Transformation of quantum states using uniformly controlled rotations. *arXiv preprint quant-ph/0407010*, 2004.
- [52] Sukin Sim, Peter D Johnson, and Alán Aspuru-Guzik. Expressibility and entangling capability of parameterized quantum circuits for hybrid quantum-classical algorithms. *Advanced Quantum Technologies*, 2(12):1900070, 2019.
- [53] Aidan Pellow-Jarman, Ilya Sinayskiy, Anban Pillay, and Francesco Petruccione. A comparison of various classical optimizers for a variational quantum linear solver. *Quantum Information Processing*, 20(6):202, 2021.
- [54] Ankit Kulshrestha and Ilya Safro. Beinit: Avoiding barren plateaus in variational quantum algorithms. In *2022 IEEE international conference on quantum computing and engineering (QCE)*, pages 197–203. IEEE, 2022.
- [55] Edward Grant, Leonard Wossnig, Mateusz Ostaszewski, and Marcello Benedetti. An initialization strategy for addressing barren plateaus in parametrized quantum circuits. *Quantum*, 3:214, 2019.
- [56] Bobak Shahriari, Kevin Swersky, Ziyu Wang, Ryan P Adams, and Nando De Freitas. Taking the human out of the loop: A review of bayesian optimization. *Proceedings of the IEEE*, 104(1):148–175, 2015.
- [57] Peter I Frazier. A tutorial on bayesian optimization. *arXiv preprint arXiv:1807.02811*, 2018.

- [58] Christopher KI Williams and Carl Edward Rasmussen. *Gaussian processes for machine learning*, volume 2. MIT press Cambridge, MA, 2006.
- [59] Benjamin Letham, Brian Karrer, Guilherme Ottoni, and Eytan Bakshy. Constrained bayesian optimization with noisy experiments. 2019.
- [60] Maximilian Balandat, Brian Karrer, Daniel Jiang, Samuel Daulton, Ben Letham, Andrew G Wilson, and Eytan Bakshy. Botorch: A framework for efficient monte-carlo bayesian optimization. *Advances in neural information processing systems*, 33:21524–21538, 2020.
- [61] Mark M Wilde. From classical to quantum shannon theory. *arXiv preprint arXiv:1106.1445*, 2011.
- [62] Pauli Virtanen, Ralf Gommers, Travis E. Oliphant, Matt Haberland, Tyler Reddy, David Cournapeau, Evgeni Burovski, Pearu Peterson, Warren Weckesser, Jonathan Bright, Stéfan J. van der Walt, Matthew Brett, Joshua Wilson, K. Jarrod Millman, Nikolay Mayorov, Andrew R. J. Nelson, Eric Jones, Robert Kern, Eric Larson, C J Carey, İlhan Polat, Yu Feng, Eric W. Moore, Jake VanderPlas, Denis Laxalde, Josef Perktold, Robert Cimrman, Ian Henriksen, E. A. Quintero, Charles R. Harris, Anne M. Archibald, Antônio H. Ribeiro, Fabian Pedregosa, Paul van Mulbregt, and SciPy 1.0 Contributors. SciPy 1.0: Fundamental Algorithms for Scientific Computing in Python. *Nature Methods*, 17:261–272, 2020.
- [63] Abeynaya Gnanasekaran and Amit Surana. Efficient variational quantum linear solver for structured sparse matrices. *arXiv preprint arXiv:2404.16991*, 2024.
- [64] Albert J Pool, Alejandro D Somoza, Conor Mc Keever, Michael Lubasch, and Birger Horstmann. Nonlinear dynamics as a ground-state solution on quantum computers. *arXiv preprint arXiv:2403.16791*, 2024.
- [65] Uri M Ascher and Linda R Petzold. *Computer methods for ordinary differential equations and differential-algebraic equations*. SIAM, 1998.

A Proofs for Sec. 5

A.1 Proof of Lem. 3

Lemma 3. *Let h be chosen such that $h\nu \leq 2$, where $\nu = \|\mathbf{A}\|_2$. Then the stiffness κ of $\tilde{\mathbf{A}}_f$ in (53) is bounded as follows*

$$\kappa(\tilde{\mathbf{A}}_f) \leq \frac{12e^{\nu T}}{h\nu}. \quad (54)$$

Proof. Let $\bar{\mathbf{A}} = \mathbf{I} + h\mathbf{A}$, and so

$$\|\bar{\mathbf{A}}\|_2 \leq 1 + h\nu,$$

where, $\nu = \|\mathbf{A}\|_2$. Using, a sequence of triangular inequalities and the submultiplicativity of $\|\cdot\|_2$, one can easily deduce

$$\|\tilde{\mathbf{A}}_f\|_2 \leq \|\mathbf{I}\|_2 + \|\bar{\mathbf{A}}\|_2 \leq 2 + h\nu. \quad (76)$$

It is easy to show that the inverse of $\tilde{\mathbf{A}}$ is composed of following blocks

$$(\tilde{\mathbf{A}}_f^{-1})_{ij} = \begin{cases} \mathbf{I} & i = j \\ \mathbf{0} & j > i \\ (\bar{\mathbf{A}})^{i-j} & j < i. \end{cases}$$

Consequently, again applying a sequence of triangular inequalities and the submultiplicativity property leads to

$$\|\tilde{\mathbf{A}}_f^{-1}\|_2 \leq \|\mathbf{I}\|_2 + \|\bar{\mathbf{A}}\|_2 + \|\bar{\mathbf{A}}^2\|_2 + \cdots + \|\bar{\mathbf{A}}^{M-1}\|_2 \leq \frac{(1 + h\nu)^M - 1}{h\nu}.$$

Thus, the condition number of $\tilde{\mathbf{A}}$ can be bounded as

$$\begin{aligned}\kappa(\tilde{\mathbf{A}}_f) &= \|\tilde{\mathbf{A}}_f\|_2 \|\tilde{\mathbf{A}}_f^{-1}\|_2 \leq (2+h\nu) \frac{(1+h\nu)^M - 1}{h\nu} \\ &\leq \frac{(2+h\nu)}{h\nu} (1+h\nu)e^{\nu T} \quad \left(\because \left(1 + \frac{a}{n}\right)^n \leq e^a \right) \\ &\leq \frac{12e^{\nu T}}{h\nu},\end{aligned}$$

where, we have used $T = (M-1)h$ and $h\nu \leq 2$. □

A.2 Proof of Lem. 4

Lemma 4. *Let $\epsilon > 0$ be the desired error, then one can choose the step size h in the forward Euler scheme (51), such that*

$$\|\mathbf{u}_c - \tilde{\mathbf{u}}_f\| \leq \epsilon, \quad (55)$$

where, \mathbf{u}_c is as defined in (47) with this selected h and $\tilde{\mathbf{u}}_f$ is solution of the system (53).

Proof. For the forward Euler scheme to be stable, the step size should satisfy

$$h \leq \frac{2}{\rho(\mathbf{A})}. \quad (77)$$

We choose $h \leq \frac{2}{\nu}$ where $\nu = \|\mathbf{A}\|_2$ which satisfies the condition (77). Furthermore, under Assumption 1 the forward Euler scheme satisfies following global error bound [65]

$$\|\mathbf{u}((k-1)h) - \hat{\mathbf{u}}_f^k\| \leq Ch, \quad k = 1, \dots, M,$$

where, $C > 0$ is a constant. It then follows that

$$\|\mathbf{u}_c - \tilde{\mathbf{u}}_f\|^2 = \sum_{k=1}^M \|\mathbf{u}((k-1)h) - \hat{\mathbf{u}}_f^k\|^2 \leq (Ch)^2(M-1),$$

which implies

$$\|\mathbf{u}_c - \tilde{\mathbf{u}}_f\| \leq Ch(M-1)^{1/2} \leq Ch^{1/2}T^{1/2}. \quad (78)$$

Thus, for any given ϵ' one can always choose

$$h < \min \left\{ \frac{(\epsilon')^2}{C^2 T}, \frac{2}{\nu} \right\},$$

such that

$$\|\mathbf{u}_c - \tilde{\mathbf{u}}_f\| \leq \epsilon',$$

and Euler scheme is stable. Finally, note that

$$\begin{aligned}\left\| \frac{\mathbf{u}_c}{\|\mathbf{u}_c\|} - \frac{\tilde{\mathbf{u}}_f}{\|\tilde{\mathbf{u}}_f\|} \right\| &\leq \left\| \frac{\mathbf{u}_c}{\|\mathbf{u}_c\|} - \frac{\tilde{\mathbf{u}}_f}{\|\mathbf{u}_c\|} + \frac{\tilde{\mathbf{u}}_f}{\|\mathbf{u}_c\|} - \frac{\tilde{\mathbf{u}}_f}{\|\tilde{\mathbf{u}}_f\|} \right\|, \\ &\leq \frac{\|\mathbf{u}_c - \tilde{\mathbf{u}}_f\|}{\|\mathbf{u}_c\|} + \frac{\|\mathbf{u}_c\| - \|\tilde{\mathbf{u}}_f\|}{\|\mathbf{u}_c\|} \leq \frac{2\|\mathbf{u}_c - \tilde{\mathbf{u}}_f\|}{\|\mathbf{u}_c\|} \leq \frac{2\epsilon'}{\|\mathbf{u}_c\|},\end{aligned} \quad (79)$$

where, we have use the fact

$$\frac{\|\|\mathbf{u}_c\| - \|\tilde{\mathbf{u}}_f\|\|}{\|\mathbf{u}_c\|} \leq \frac{\|\mathbf{u}_c - \tilde{\mathbf{u}}_f\|}{\|\mathbf{u}_c\|}.$$

Thus, for given ϵ , by choosing $\epsilon' = \|\mathbf{u}_c\|\epsilon/2$ and determining h as described above, we can conclude

$$\left\| \frac{\mathbf{u}_c}{\|\mathbf{u}_c\|} - \frac{\tilde{\mathbf{u}}_f}{\|\tilde{\mathbf{u}}_f\|} \right\| \leq \epsilon,$$

as required. □

A.3 Proof of Thm. 2

Theorem 2. Consider the IVP (46) under Assumption 1. Additionally, assume that \mathbf{A} in (46) is a normal matrix. Let $0 < \epsilon < 1$ be the desired solution accuracy, then one can choose the step size h in the forward Euler scheme (51), and γ the stopping threshold in VQLS algorithm (2) such that

$$\|\mathbf{u}_c\rangle - |\bar{\mathbf{u}}_f\rangle\| \leq \epsilon, \quad (64)$$

where, $|\bar{\mathbf{u}}_f\rangle = \mathbf{V}(\theta^*)|\mathbf{0}\rangle$ is solution generated by applying VQLS to the linear system (53). Furthermore, under the Assumption 2 the query complexity scales as

$$\mathcal{O}\left(\log^{8.5}\left(\frac{NT^4}{\|\mathbf{u}_c\|^2\epsilon^2}\right)\frac{T^3}{\|\mathbf{u}_c\|^2\epsilon^2}\log(1/\epsilon)\right). \quad (65)$$

Proof. Given \mathbf{A} is a normal matrix i.e. $\mathbf{A}^*\mathbf{A} = \mathbf{A}\mathbf{A}^*$, it can always be decomposed into the form $\mathbf{A} = \mathbf{V}^T\Lambda\mathbf{V}$ where \mathbf{V} is an unitary matrix and Λ is a diagonal matrix with diagonal entries as the eigenvalues of \mathbf{A} . Then

$$\|\mathbf{I} + h\mathbf{A}\|_2 = \|\mathbf{V}^T(\mathbf{I} + h\Lambda)\mathbf{V}\|_2 \leq \rho(\mathbf{I} + h\Lambda).$$

We choose h such that $\rho(\mathbf{I} + h\Lambda) \leq 1$, or

$$|1 + h\lambda_j|^2 \leq 1,$$

for all λ_j eigenvalues of \mathbf{A} . Let, $\lambda_j = -\delta_j + i\omega_j$ where $\delta_j > 0$ (or $\delta_j \geq 0$ if $\omega_j = 0$) by Assumption 1, then above condition can be met by choosing

$$h \leq \min_j \frac{2\delta_j}{|\lambda_j|^2},$$

Thus, for

$$h \leq h_0 \equiv \min_j \left\{ \frac{2\delta_j}{|\lambda_j|^2}, \frac{2}{\max_k |\lambda_k|} \right\}, \quad (80)$$

following holds

$$\|\mathbf{I} + h\mathbf{A}\|_2 \leq 1, \quad (81)$$

and the condition for stability of forward Euler is also satisfied.

Euler error: We next revisit error bounds for forward Euler under the assumption (81). By Taylor expansion

$$\mathbf{u}((k+1)h) = \mathbf{u}(kh) + h\mathbf{A}\mathbf{u}(kh) + h\mathbf{b}(kh) + \tau_k,$$

where, τ_k is the local truncation error which can be expressed as

$$\|\tau_k\| \leq \frac{M_k}{2}h^2, \quad (82)$$

under the Assumptions 1, where $M_k > 0$ is a constant. Thus

$$\mathbf{u}(kh) - \hat{\mathbf{u}}_f^{k+1} = \mathbf{u}((k-1)h) + h\mathbf{A}\mathbf{u}((k-1)h) + h\mathbf{b}((k-1)h) + \tau_k - (\hat{\mathbf{u}}_f^k + h\mathbf{A}\hat{\mathbf{u}}_f^k + h\mathbf{b}((k-1)h)),$$

which implies the norm of the error $e_k = \|\mathbf{u}((k-1)h) - \hat{\mathbf{u}}_f^k\|$ satisfies

$$e_{k+1} \leq \|(\mathbf{I} + h\mathbf{A})\|e_k + \|\tau_k\|. \quad (83)$$

Iterating on k we get

$$e_{k+1} \leq \|(\mathbf{I} + h\mathbf{A})\|^k e_1 + (\|(\mathbf{I} + h\mathbf{A})\|^{k-1}\|\tau_1\| + \|(\mathbf{I} + h\mathbf{A})\|^{k-2}\|\tau_2\| + \dots\|\tau_k\|). \quad (84)$$

Since $e_1 = 0$ for Euler method, using the condition (81) and (82) for some constant $C > 0$, we conclude that

$$\|\mathbf{u}((k-1)h) - \hat{\mathbf{u}}_f^k\| = e_k \leq C(k-1)h^2.$$

It then follows that

$$\|\mathbf{u}_c - \tilde{\mathbf{u}}_f\|^2 = \sum_{k=1}^M \|\mathbf{u}((k-1)h) - \hat{\mathbf{u}}_f^k\|^2 \leq (Ch^2)^2 \sum_{k=1}^M (k-1)^2,$$

which implies

$$\|\mathbf{u}_c - \tilde{\mathbf{u}}_f\| \leq Ch^2(M-1)^{3/2} \leq Ch^{1/2}T^{3/2}. \quad (85)$$

Thus, for any given ϵ' one can choose

$$h < \min \left\{ \frac{(\epsilon')^2}{C^2T^3}, h_0 \right\}, \quad (86)$$

where h_0 is as defined in (80), so that

$$\|\mathbf{u}_c - \tilde{\mathbf{u}}_f\| \leq \epsilon'.$$

Finally, for given ϵ , by choosing $\epsilon' = \|\mathbf{u}_c\|\epsilon/2$, selecting h as described above, and following the steps in the Lemma 4, we conclude

$$\left\| \frac{\mathbf{u}_c}{\|\mathbf{u}_c\|} - \frac{\tilde{\mathbf{u}}_f}{\|\tilde{\mathbf{u}}_f\|} \right\| \leq \epsilon.$$

Condition number: Under the condition (81), following similar steps as in the proof of the Lemma 3, one can deduce

$$\|\tilde{\mathbf{A}}_f\|_2 \leq \|\mathbf{I}\|_2 + \|\overline{\mathbf{A}}\|_2 \leq 2,$$

and

$$\|\tilde{\mathbf{A}}_f^{-1}\|_2 \leq \|\mathbf{I}\|_2 + \|\overline{\mathbf{A}}\|_2 + \|\overline{\mathbf{A}}^2\|_2 + \cdots + \|\overline{\mathbf{A}}^{M-1}\|_2 \leq M,$$

where we used the fact that $\|\overline{\mathbf{A}}^k\|_2 \leq (\|\overline{\mathbf{A}}\|_2)^k \leq 1$ for $k = 1, 2, \dots, M-1$. Thus, the condition number of $\tilde{\mathbf{A}}_f$ can be bounded as

$$\kappa(\tilde{\mathbf{A}}_f) = \|\tilde{\mathbf{A}}_f\|_2 \|\tilde{\mathbf{A}}_f^{-1}\|_2 \leq 2M.$$

Finally, choose

$$h < \min \left\{ \frac{(\epsilon\|\mathbf{u}_c\|)^2}{16C^2T^3}, h_0 \right\}, \quad (87)$$

and

$$\gamma = \frac{1 - (1 - \frac{\epsilon^2}{8})^2}{2(2M)^2 \log(NM)} < 1, \quad (88)$$

and follow steps similar to the proof of Thm. 1 to conclude that

$$\|\langle \mathbf{u}_c \rangle - \langle \tilde{\mathbf{u}}_f \rangle\| \leq \epsilon. \quad (89)$$

Furthermore, under Assumption 2 the query complexity can be determined as follows

$$\begin{aligned} & \mathcal{O}(\log^{8.5}(NM)\kappa \log(1/\epsilon')) = \mathcal{O}(\log^{8.5}(NT/h)2(T/h) \log(1/\epsilon)) \\ & = \mathcal{O}\left(\log^{8.5}\left(NT\left(\frac{1}{h_0} + \frac{4C^2T^3}{\|\mathbf{u}_c\|^2\epsilon^2}\right)\right)\left(\frac{1}{h_0} + \frac{4C^2T^3}{\|\mathbf{u}_c\|^2\epsilon^2}\right) \log(1/\epsilon)\right) \\ & = \mathcal{O}\left(\log^{8.5}\left(\frac{NT^4}{\|\mathbf{u}_c\|^2\epsilon^2}\right) \frac{T^3}{\|\mathbf{u}_c\|^2\epsilon^2} \log(1/\epsilon)\right), \end{aligned}$$

where, we have assumed $\mathcal{O}(h_0) = 1$.

□

A.4 Proof of Lem. 5

Lemma 5. *Let h be chosen such that $h\nu \leq 0.5$, where $\nu = \|\mathbf{A}\|$. Then the stiffness κ of $\tilde{\mathbf{A}}_b$ in (69) is bounded as follows*

$$\kappa(\tilde{\mathbf{A}}_b) \leq 2.5(T/h + 1), \quad (70)$$

if $\|(\mathbf{I} - h\mathbf{A})^{-1}\| \leq 1$ or

$$\kappa(\tilde{\mathbf{A}}_b) \leq \frac{5e^{2\nu T}}{h\nu}, \quad (71)$$

if $\|(\mathbf{I} - h\mathbf{A})^{-1}\| > 1$.

Let $\bar{\mathbf{A}} = \mathbf{I} - h\mathbf{A}$, and so

$$1 \leq \|\bar{\mathbf{A}}\|_2 \leq 1 + h\nu,$$

where, $\nu = \|\mathbf{A}\|_2$ and we have used the fact that $\|\bar{\mathbf{A}}\|_2 \geq \rho(\mathbf{I} - h\mathbf{A}) \geq 1$ based on Assumption 1. Using, a sequence of triangular inequalities and the submultiplicativity of $\|\cdot\|_2$, one can easily deduce

$$\|\tilde{\mathbf{A}}_b\|_2 \leq \|\mathbf{I}\|_2 + \max\{\|I\|_2, \|\bar{\mathbf{A}}\|_2\} \leq 1 + \|\bar{\mathbf{A}}\|_2 \leq 2 + h\nu.$$

Next note that $(\mathbf{I} - h\mathbf{A})$ is invertible since its eigenvalues $\frac{1}{1-h\lambda}$ are non-zero under Assumption 1, condition A1. Using the matrix inversion lemma, we get

$$(\mathbf{I} - h\mathbf{A})^{-1} = \sum_{k=0}^{\infty} (h\mathbf{A})^k,$$

and implies

$$\|\bar{\mathbf{A}}^{-1}\| = \|(\mathbf{I} - h\mathbf{A})^{-1}\| \leq \frac{1}{1-h\nu} \leq 1 + 2h\nu, \quad (90)$$

assuming h is chosen such that $h\nu < 0.5$.

It can be shown that the inverse of $\tilde{\mathbf{A}}_b$ is composed of following blocks

$$(\tilde{\mathbf{A}}_b^{-1})_{ij} = \begin{cases} (\bar{\mathbf{A}}^{-1})^{i-1} & j = 1 \\ \bar{\mathbf{A}}^{-1} & i = j, j \neq 1 \\ (\bar{\mathbf{A}}^{-1})^{(i-j)+1} & i > j, j \neq 1 \end{cases}.$$

Consequently, applying a sequence of triangular inequalities and using the submultiplicative property leads to

$$\|\tilde{\mathbf{A}}_b^{-1}\|_2 \leq \max\{\|I\|_2, \|\bar{\mathbf{A}}^{-1}\|_2\} + \max\{\|\bar{\mathbf{A}}^{-1}\|_2, \|\bar{\mathbf{A}}^{-2}\|_2\} + \dots + \max\{\|\bar{\mathbf{A}}^{-(M-2)}\|_2, \|\bar{\mathbf{A}}^{-(M-1)}\|_2\} + \|\bar{\mathbf{A}}^{-(M-1)}\|_2.$$

We consider two cases.

Case 1: $\|\bar{\mathbf{A}}^{-1}\| \leq 1$, which implies $\|\bar{\mathbf{A}}^{-k}\| \leq 1$

$$\|\tilde{\mathbf{A}}_b^{-1}\|_2 \leq M.$$

Thus, the condition number of $\tilde{\mathbf{A}}_b$ can be bounded as

$$\kappa(\tilde{\mathbf{A}}_b) = \|\tilde{\mathbf{A}}_b\|_2 \|\tilde{\mathbf{A}}_b^{-1}\|_2 \leq (2 + h\nu)M \leq 2.5(T/h + 1), \quad (91)$$

where, we have used $T = (M - 1)h$ and assumed $h\nu < 0.5$.

Case 2: $\|\bar{\mathbf{A}}^{-1}\| > 1$, which implies

$$\begin{aligned} \|\tilde{\mathbf{A}}_b^{-1}\|_2 &\leq \|\bar{\mathbf{A}}^{-1}\|_2 + \|\bar{\mathbf{A}}^{-2}\|_2 + \dots + \|\bar{\mathbf{A}}^{-(M-1)}\|_2 + \|\bar{\mathbf{A}}^{-M}\|_2 \\ &\leq (1 + 2h\nu) \frac{(1 + 2h\nu)^M}{2h\nu} \leq \frac{(1 + 2h\nu)^2}{2h\nu} e^{2\nu T} \\ &\leq \frac{2}{h\nu} e^{2\nu T}. \end{aligned}$$

Thus, condition number of $\tilde{\mathbf{A}}_b$ can be bounded as

$$\kappa(\tilde{\mathbf{A}}_b) \leq (2 + h\nu) \frac{2}{h\nu} e^{2\nu T} \leq \frac{5}{h\nu} e^{2\nu T}. \quad (92)$$

A.5 Proof of Lem. 6

Lemma 6. Let $\epsilon > 0$ be the desired error, the one can choose the step size h in implicit Euler scheme (67), such that

$$\|\mathbf{u}_c - \tilde{\mathbf{u}}_b\| \leq \epsilon, \quad (72)$$

where, \mathbf{u}_c is as defined in (47) with this selected h and $|\tilde{\mathbf{u}}_b\rangle$ is solution of the system (69).

Under the Assumptions 1, the backward Euler scheme is stable. For backward Euler, the error equation is

$$\mathbf{u}(kh) - \hat{\mathbf{u}}_b^{k+1} = \mathbf{u}((k-1)h) + h\mathbf{A}\mathbf{u}(kh) + h\mathbf{b}(kh) + \tau_k - (\hat{\mathbf{u}}_b^k + h\mathbf{A}\hat{\mathbf{u}}_b^{k+1} + h\mathbf{b}(kh)),$$

which implies the norm of the error $e_k = \|\mathbf{u}((k-1)h) - \hat{\mathbf{u}}_b^k\|$ satisfies

$$e_{k+1} \leq \|(\mathbf{I} - h\mathbf{A})^{-1}\| (e_k + \|\tau_k\|), \quad (93)$$

where, as before the local truncation error τ_k satisfies $\|\tau_k\| \leq \frac{M_k h^2}{2}$ for $M_k \geq 0$.

As in Lemma 5, we consider two cases under the assumption $h\nu < 0.5$.

Case I: $\|(\mathbf{I} - h\mathbf{A})^{-1}\| \leq 1$ under which backward scheme satisfies following global error bound

$$\|\mathbf{u}((k-1)h) - \hat{\mathbf{u}}_b^k\| \leq C_1 h^2 (k-1),$$

where, $C_1 > 0$ is a constant. Thus, following similar steps as in the proof of Theorem 2, for any given ϵ one can choose

$$h < \min \left\{ \frac{(\epsilon \|\mathbf{u}_c\|)^2}{4C_1^2 T^3}, \frac{0.5}{\nu} \right\}, \quad (94)$$

such that

$$\left\| \frac{\mathbf{u}_c}{\|\mathbf{u}_c\|} - \frac{\tilde{\mathbf{u}}_b}{\|\tilde{\mathbf{u}}_b\|} \right\| \leq \epsilon'. \quad (95)$$

Case II: $\|(\mathbf{I} - h\mathbf{A})^{-1}\| > 1$ under which backward scheme satisfies following global error bound

$$\|\mathbf{u}((k-1)h) - \hat{\mathbf{u}}_b^k\| \leq C_2 h,$$

where, $C_2 > 0$ is a constant. Thus, following similar steps as in the Lemma 4, for any given ϵ one can choose

$$h < \min \left\{ \frac{(\epsilon \|\mathbf{u}_c\|)^2}{4C_2^2 T}, \frac{0.5}{\nu} \right\} \quad (96)$$

such that (95) holds.